AD-A082 800 GENERAL ELECTRIC CO ALBUQUERQUE N MEX TEMPO F/G 20/8
PHOTOGRAMMETRY OF THE PARTICLE TRAJECTORIES ON DIPOLE WEST SHOT--ETC(U)
NOV 79 J M DEWEY, D J MCMILLIN DNA001-77-C-0305
UNCLASSIFIED DNA-4326F-5 NL

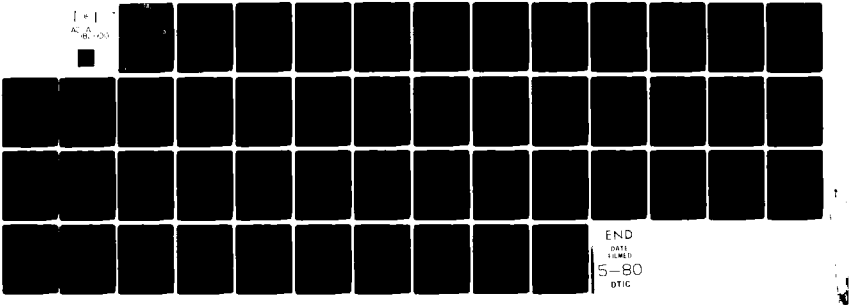

END
DATE FILMED
5-80
DTIC

(12) LEVEL III

AD-E 300 699

DNA 4326F-5

ADA082800

PHOTOGRAMMETRY OF THE PARTICLE TRAJECTORIES ON DIPOLE WEST SHOTS 8, 9, 10, AND 11

Volume V—Comparison of Results

J.M. Dewey
D.J. McMillin
University of Victoria
British Columbia
Canada V8W 2Y2

DTIC
ELECTE
APR 8 1980
S D
B

30 November 1979

Final Report for Period 1 March 1978—30 November 1978

CONTRACT No. DNA 001-77-C-0305

APPROVED FOR PUBLIC RELEASE;
DISTRIBUTION UNLIMITED.

THIS WORK SPONSORED BY THE DEFENSE NUCLEAR AGENCY
UNDER RDT&E RMSS CODE B342077464 N99QAXAA11114 H2590D.

DDC FILE COPY

Prepared for
Director
DEFENSE NUCLEAR AGENCY
Washington, D. C. 20305

80 3 5 012

Destroy this report when it is no longer needed. Do not return to sender.

PLEASE NOTIFY THE DEFENSE NUCLEAR AGENCY, ATTN: STTI, WASHINGTON, D.C. 20305, IF YOUR ADDRESS IS INCORRECT, IF YOU WISH TO BE DELETED FROM THE DISTRIBUTION LIST, OR IF THE ADDRESSEE IS NO LONGER EMPLOYED BY YOUR ORGANIZATION.

UNCLASSIFIED

SECURITY CLASSIFICATION OF THIS PAGE *(When Data Entered)*

REPORT DOCUMENTATION PAGE

READ INSTRUCTIONS BEFORE COMPLETING FORM

1. REPORT NUMBER: DNA 4326F-5
2. GOVT ACCESSION NO.:
3. RECIPIENT'S CATALOG NUMBER:

4. TITLE *(and Subtitle)*: PHOTOGRAMMETRY OF THE PARTICLE TRAJECTORIES ON DIPOLE WEST SHOTS 8, 9, 10, AND 11 Volume V—Comparison of Results

5. TYPE OF REPORT & PERIOD COVERED: Final Report for Period 1 Mar 78—30 Nov 78

6. PERFORMING ORG. REPORT NUMBER:

7. AUTHOR(s): J. M. Dewey, D. J. McMillin

8. CONTRACT OR GRANT NUMBER(s): DNA001-77-C-0305

9. PERFORMING ORGANIZATION NAME AND ADDRESS: University of Victoria, British Columbia, Canada V8W 2Y2

10. PROGRAM ELEMENT, PROJECT, TASK AREA & WORK UNIT NUMBERS: NWED Subtask N99QAXAA111-14

11. CONTROLLING OFFICE NAME AND ADDRESS: Director, Defense Nuclear Agency, Washington, D.C. 20305

12. REPORT DATE: 30 November 1979

13. NUMBER OF PAGES: 50

14. MONITORING AGENCY NAME & ADDRESS *(if different from Controlling Office)*: General Electric Company—TEMPO, 7800 Marble Avenue NE, Suite 5, Albuquerque, New Mexico 87110

15. SECURITY CLASS *(of this report)*: UNCLASSIFIED

15a. DECLASSIFICATION DOWNGRADING SCHEDULE:

16. DISTRIBUTION STATEMENT *(of this Report)*

Approved for public release; distribution unlimited.

62707

17. DISTRIBUTION STATEMENT *(of the abstract entered in Block 20, if different from Report)*

18 SUPPLEMENTARY NOTES

This work sponsored by the Defense Nuclear Agency under RDT&E RMSS Code B342077464 N99QAXAA11114 H2590D.

19 KEY WORDS *(Continue on reverse side if necessary and identify by block number)*

Photogrammetric Analysis
Particle Trajectories
Air Particle Tracers
Simultaneous Detonations
Multiburst Detonations
Mach Stem Shock Waves

20 ABSTRACT *(Continue on reverse side if necessary and identify by block number)*

Volume V, the final volume of this series, compares the results obtained by photogrammetry of smoke-puff particle flow tracers in four experiments (DIPOLE WEST Shots 8 to 11) involving the simultaneous detonation of pairs of 1080-lb (490-kg) Pentolite charges. In Shots 8 and 11, one charge was at a height of 25 feet (7.6m) above the ground, and the second charge was 50 feet (15.2m) above the first. The corresponding distances for Shots 9 and 10 were 15 feet (4.6m) and 30 feet (9.2m). For Shots 8 and 9, the ground surface was

DD FORM 1 JAN 73 1473 EDITION OF 1 NOV 65 IS OBSOLETE

UNCLASSIFIED

SECURITY CLASSIFICATION OF THIS PAGE *(When Data Entered)*

20. ABSTRACT (Continued)

smooth, and for Shots 10 and 11, the ground close to the charges was roughened by ploughing to a depth of approximately 14 inches (35 cm). The analysis of the photographically observed particle trajectories in the blast waves of each experiment provided information on the strengths of the primary and Mach stem shock waves, and a measure of the space and time variations of particle velocity, density, hydrostatic overpressure and dynamic pressure in the blast waves. Comparisons between these results from the four experiments show complete consistency in the trajectories of the primary shocks from all eight charges, indicating that they all detonated satisfactorily with equal energy yields. The measurements of the Mach stem blast waves above and below the horizontal interaction planes between the pairs of charges provide a set of "ideal" values against which to compare blast wave reflections from real ground surfaces. The blast wave profiles in the "ideal" Mach stems for the two heights of burst are very similar at equal distances from the ground zero axis. The observed differences between the Mach stem shock strengths above the ground and at the interaction plane are similar to, but not as large as those observed close to the ground using refractive image analysis. This implies both a height dependence for shock strength and variability in the shape of the Mach stem shock. Comparisons between the profiles of the blast waves over the ground and along the interaction plane show a consistent pattern in which the velocity, density and pressure immediately behind the shock above the ground are normally less than that at the interaction plane, but in which these values at later times are larger above the ground than at the interaction plane. This effect may be due to a lack of symmetry in the dipole experiments and not to ground surface effects.

SUMMARY

This is the final volume in a series which represents the particle trajectory analysis results from four experiments (DIPOLE WEST Shots 8, 9, 10 and 11) carried out to obtain information on the interaction of spherical blast waves with real and ideal reflecting surfaces. In each experiment, two 1080-pound (490-kg) Pentolite charges were detonated simultaneously. For Shots 8 and 11, the first charge was positioned at a height of 25 feet (7.6 m) above the ground surface, and the second charge 50 feet (15.2 m) above the first. The corresponding distances for Shots 9 and 10 were 15 feet (4.6 m) and 30 feet (9.2 m). For Shots 8 and 9, the ground surface was smooth, and for Shots 10 and 11, the ground surface in the region close to the charges was roughened by plowing to a depth of approximately 14 inches (35 cm).

In each experiment, high-speed photographic records were made of the movements of smoke-puff particle tracers in a region adjacent to the charges. The observed trajectories of the particle tracers were analyzed to provide the following information: the trajectories of the primary and Mach stem shock fronts; the variation of shock strength with distance; the particle velocity, density, hydrostatic overpressure and dynamic pressure fields at specific times after charge detonation; and time histories of these physical properties at fixed locations in the region of the smoke puff grid. The results for each of the four experiments were reported in the preceding volumes of this series. In this volume, the results from the four experiments are compared. It is shown that there is complete consistency in the trajectories of the primary shocks from all eight explosions, indicating that each charge detonated satisfactorily and all yielded identical amounts of energy.

Comparisons between the variation of Mach stem shock strength with distance over the ground and along the interaction plane between the two charges show that the shock strength over the rough ground was significantly less than that at the interaction plane or over smooth ground. This is consistent with the results obtained previously from refractive image studies of the shock waves. The measurements of the Mach stem blast waves above and below the interaction plane provide a set of "ideal" values against which to compare results of blast wave reflections from real ground surfaces. The results obtained from the particle trajectory analysis include the variation of Mach stem shock strength with distance, and the space and time variations of particle velocity, density, hydrostatic overpressure and dynamic pressure.

Comparisons of the blast wave profiles in the ideal Mach stems for the two heights of burst show little difference in the profiles at equal distances from the ground zero axis. Comparisons between the profiles of the blast waves over the ground and along the interaction plane show a consistent pattern in which the value immediately behind the shock above the ground is less than at the interaction plane, but in which at later times the values above the ground are larger than those at the interaction plane. This effect may be due to a lack of symmetry in the dipole experiments.

PREFACE

The authors gratefully acknowledge the opportunity offered by Defence Research Establishment Suffield and Defense Nuclear Agency to participate in the experiments described in this report. The analyses described here were carried out under contract with Canadian General Electric Company and with additional financial support from a research grant by the National Research Council (A2952).

The advice and assistance of Mr. A.P. Lambert, Canadian General Electric Project Officer at DRES, Dr. L. Kennedy of General Electric Company—TEMPO, and Mr. J. Keefer of the Ballistic Research Laboratories are also gratefully acknowledged.

UNIT CONVERSION AND SCALING FACTORS

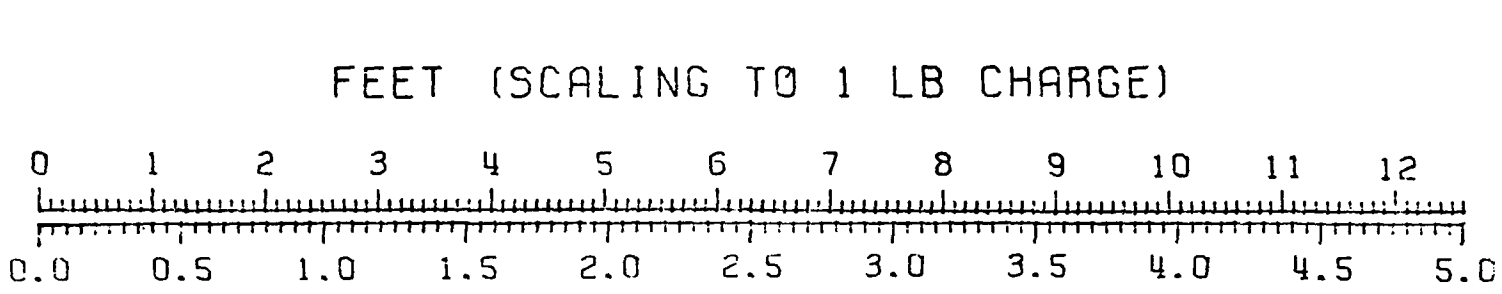

For feet scaled to a 1000-lb charge, multiply the top scale by 10.

For time scaled to a 1000-lb charge, multiply time scaled to a 1-kg charge by 8.683.

For pressure in kPa, multiply a pressure ratio (in atmospheres) by 101.325. For pressure in psi, multiply the pressure ratio by 14.696. To convert kPa to psi, divide by 6.895.

To obtain the values of distance, time and pressure actually observed in any experiment, multiply scaled values in this report by the appropriate factor from the following table:

Shot Number	Distance (m)	Distance (ft)	Time (ms)	Pressure (kPa)	Pressure (psi)
8	8.1051	26.591	8.0262	93.22	13.52
9	8.1111	26.611	8.1069	93.02	13.49
10	8.0718	26.482	8.3742	94.38	13.69
11	8.0730	26.485	8.5933	94.34	13.68

TABLE OF CONTENTS

LIST OF ILLUSTRATIONS

SECTION 1

INTRODUCTION

1-1 DEFINITION OF EXPERIMENTS.

This volume presents the particle trajectory analysis results from four experiments (DIPOLE WEST Shots 8, 9, 10 and 11), carried out to obtain information on the interaction of spherical blast waves with real and ideal reflecting surfaces. A general description of the experiments and of the methods used to analyze the photographically observed particle trajectories can be found in Volume I of this series. The results of the particle trajectory analysis from the four experiments, which were presented in Volumes I through IV, are compared and summarized in the present volume.

In each experiment, two 1080-pound (490-kg) Pentolite charges were detonated simultaneously. For Shots 8 and 11, the first charge was positioned at a height of 25 feet (7.6 m) above the ground surface, and the second charge 50 feet (15.2 m) above the first. The corresponding distances for Shots 9 and 10 were 15 feet (4.6 m) and 30 feet (9.2 m). For Shots 8 and 9, the ground surface was smooth, and for Shots 10 and 11, the ground surface in the region around the charges was roughened by plowing, to a depth of approximately 14 inches (35 cm).

In each experiment, photogrammetrical studies were made of the shock fronts (refractive image analysis, RIA) and of the motions of smoke-puff particle tracers (particle trajectory analysis, PTA). The refractive image analysis results were reported by Dewey et al (1975). In each of the preceding volumes of this series, the following particle trajectory analysis results were presented: the trajectories of the primary and Mach stem shock fronts as derived from particle trajectory time-of-arrival data, and the subsequently derived variation of shock strength with distance in each case; contours showing the particle velocity, density, hydrostatic overpressure, and dynamic pressure fields at specific times after charge detonation; and time histories of these physical properties at fixed locations in the region of the smoke puff grid. The results described above from the four experiments are compared in the next two sections of the present volume. A final section summarizes the comparisons and presents conclusions.

1-2 METHOD OF COMPARISON.

To permit the comparison of the results from the four experiments, which were carried out in a variety of atmospheric conditions, the results of each experiment were scaled to represent a pair of 1 kg charges detonated in a standard atmosphere of dry air at 15°C at sea level. The details of the scaling procedure are given in the preceding volumes.

Results are presented in SI units, although the experiments were originally laid out in British units. Only distance and time measurements are affected as velocity, density and pressure results are presented in dimensionless ratios. A distance units conversion scale is included on page 4 to convert between SI units (meters scaled to a 1 kg charge) and British units (feet scaled to a 1-pound charge), plus factors to convert distances and times to a 1000-pound charge in a standard atmosphere, and factors to convert pressure ratios to both British and SI pressure units. Scale factors which may be used to compute the distance and time values actually observed under the ambient conditions of each shot are also provided.

SECTION 2

COMPARISON OF SHOCK FRONT STRENGTHS

2-1 PRIMARY SHOCK FRONTS.

The radius-time trajectories of the primary shock fronts from each of the eight charges used in the four experiments—DIPOLE WEST Shots 8 through 11—are shown in Figure 1. The time of arrival of each shock front at each smoke puff was obtained from the high-speed films of the smoke puff movements to provide a series of values for shock radius and time. The agreement between the results shown in Figure 1, especially in the slope of the trajectories, confirms the uniformity of energy release in each of the eight original explosions.

For the upper charges used in these experiments, good primary shock-front trajectory data were obtained, using only particle trajectory analysis since no data were available from the refractive image analysis and very few from pressure gauge measurements. Because of the charge configurations used, more data were obtained for the upper charges on Shots 9 and 10 than on Shots 8 and 11. On the other hand, fewer trajectory data were obtained for Shots 9 and 10 for the primary shock fronts from the lower charges. The most complete set of primary data (both PTA and RIA) was obtained for the lower charges on Shots 8 and 11.

The shock trajectory data shown in Figure 1 were analyzed to determine the variation of shock strength with distance, in a manner described in Volume I of this series. Results of this analysis for each of the eight primary shock fronts were presented separately in the earlier volumes. Like the shock trajectory data presented in Figure 1, the shock strength results for each charge showed good agreement, except for the lower charges on Shots 9 and 10, where the data were too few to permit a reliable analysis of the shock velocity. The primary shock strength results presented in the earlier volumes also showed good agreement with similar results obtained using refractive image analysis on the opposite side of the charges.

Because of the agreement between the primary shock-front trajectory data from all eight charges, the data were combined and analyzed together. The combined radius-time data-fit is shown in Figure 1 as a smooth curve. The variation with distance from the charge center of primary shock-front strength (in

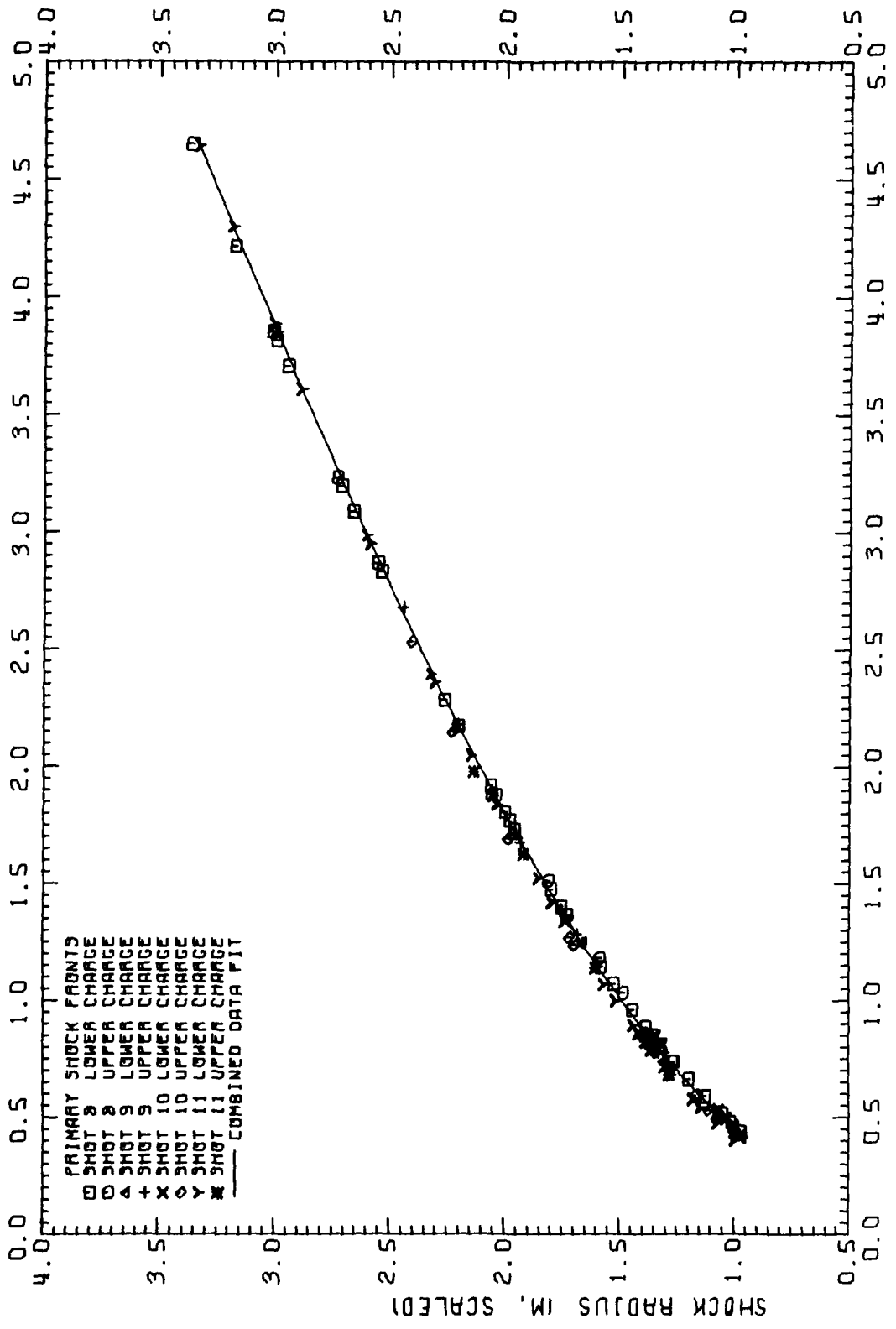

Figure 1. Primary shock-front trajectories.

terms of shock Mach number), using the combined data shown in Figure 1, is given in Figure 2. A separate scale gives the shock strength in terms of the overpressure ratio across the shock front.

Also plotted in Figure 2 are points from the combined refractive image analysis of Shots 8 through 11. These data were obtained by photographing the shock fronts against a striped backdrop on the opposite side of the charges to the smoke puffs. The RIA results for the four experiments were compared in detail by Dewey et al (1975), and agreement between experiments was found to be good.

2-2 MACH STEM SHOCKS ABOVE AND BELOW THE INTERACTION PLANE.

The dipole experiments were designed with the postulate that the Mach stem shocks produced above and below the plane of symmetry between the two charges would involve no loss or redistribution of energy, and would therefore represent the reflection of a spherical shock from an ideal reflecting surface. The radius-time trajectory data for the Mach stem shocks above and below the interaction plane in Shots 8 and 11, obtained using particle trajectory analysis, are plotted in Figure 3. Again, the results from the four shock fronts are very similar, and these data were combined and analyzed together. The combined fit is shown as a smooth curve in Figure 3.

Figure 4 shows the variation of shock strength with distance for the four interaction Mach stems on Shots 8 and 11, computed using the combined particle trajectory analysis data in a manner similar to that described for the primary shock fronts. Also shown is the variation of shock strength, computed using the combined refractive image analysis data for the Mach stems below the interaction plane, reported by Dewey et al (1975). No data were available above the interaction plane from the refractive image analysis.

Agreement between the interaction Mach stem results for the two experiments, and using the two measurement techniques, is good in spite of the uncertainty about the shape of the Mach stem shocks, a problem discussed in the earlier volumes. For refractive image analysis of the Mach stem shocks, the shock positions were measured very close to the interaction plane, and distances were measured along the interaction plane from the point where the axis joining the two charge centers cut the plane. In the smoke puff analysis,

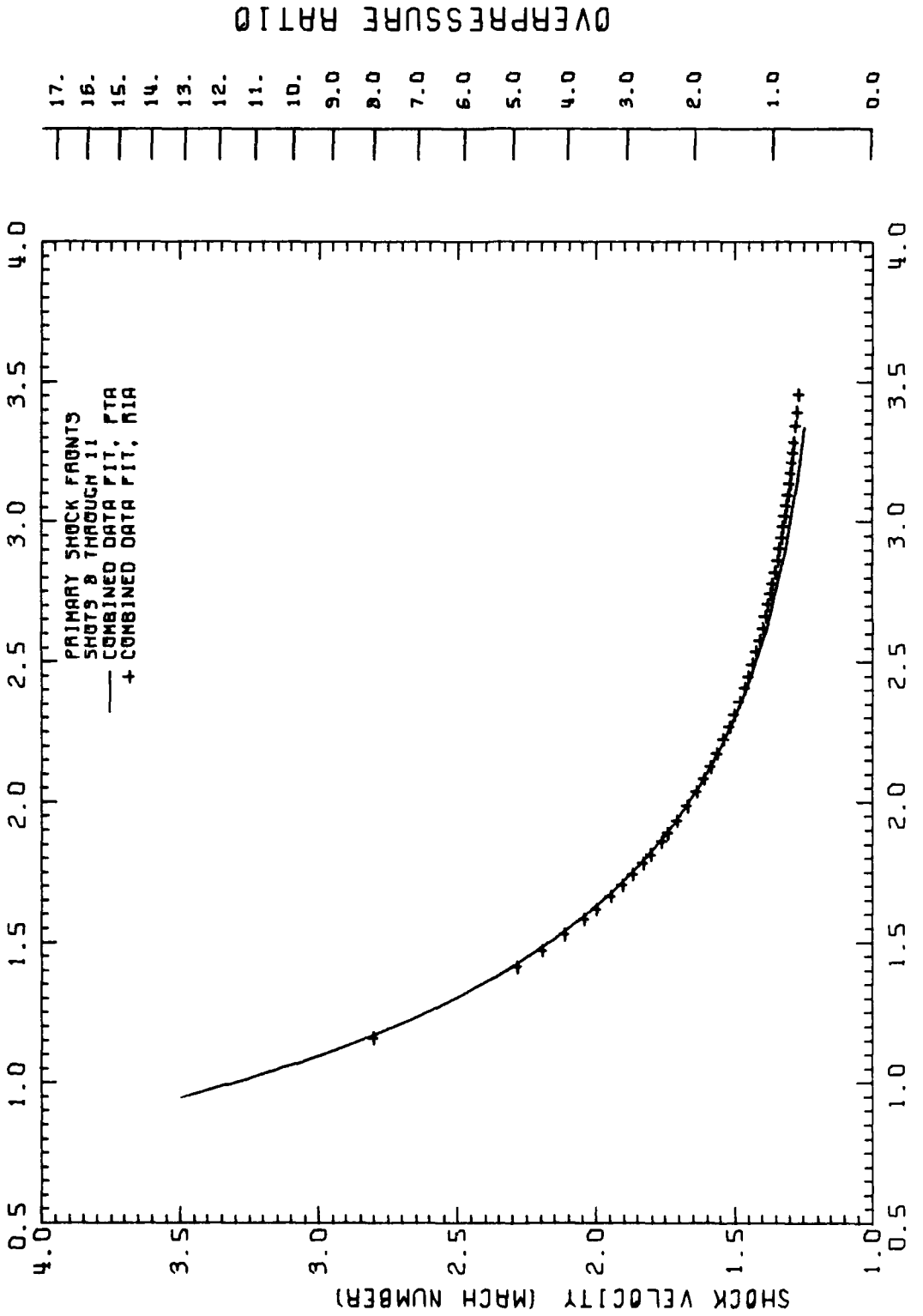

Figure 2. Primary shock-front strengths.

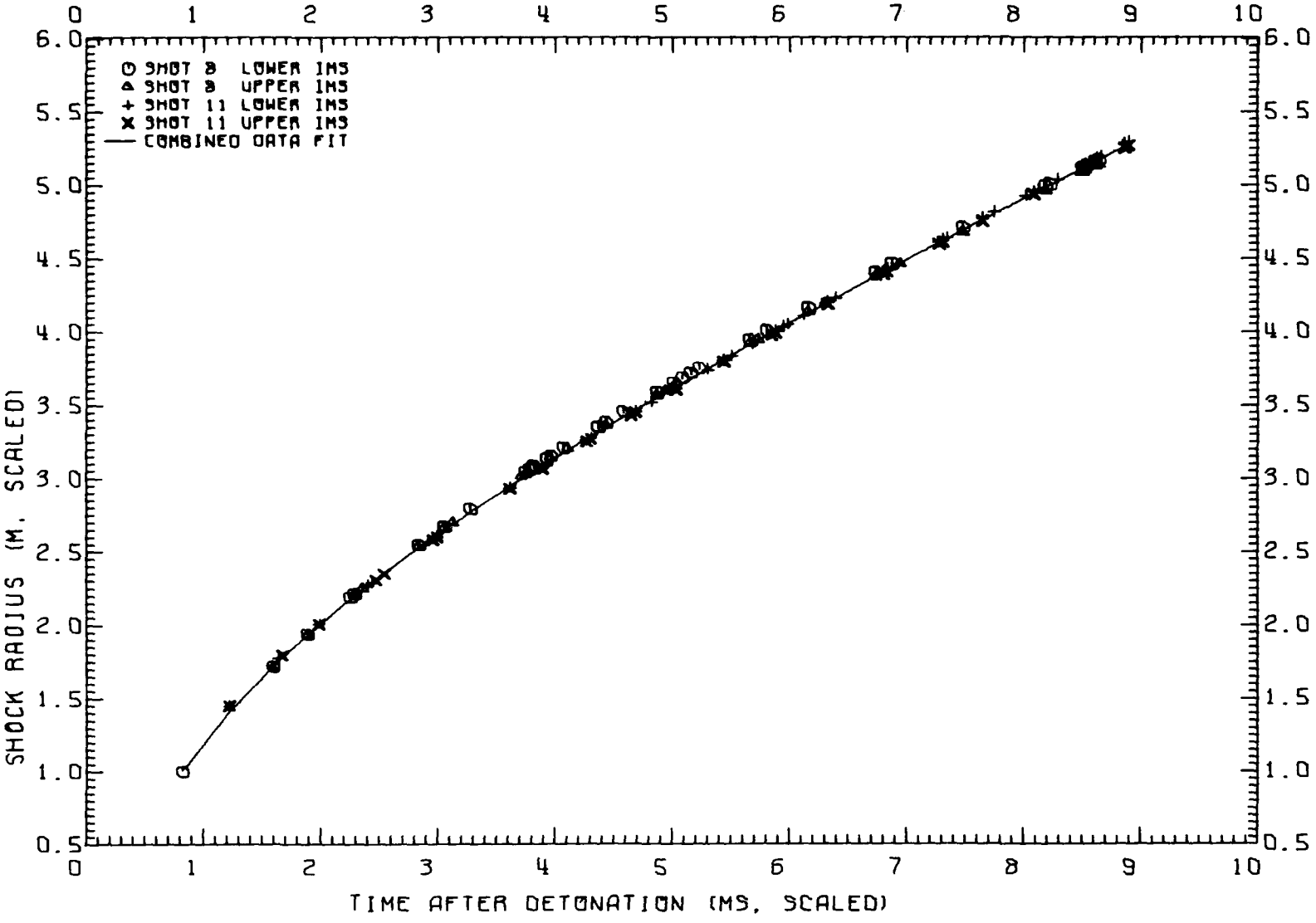

Figure 3. Interaction Mach stem trajectories.

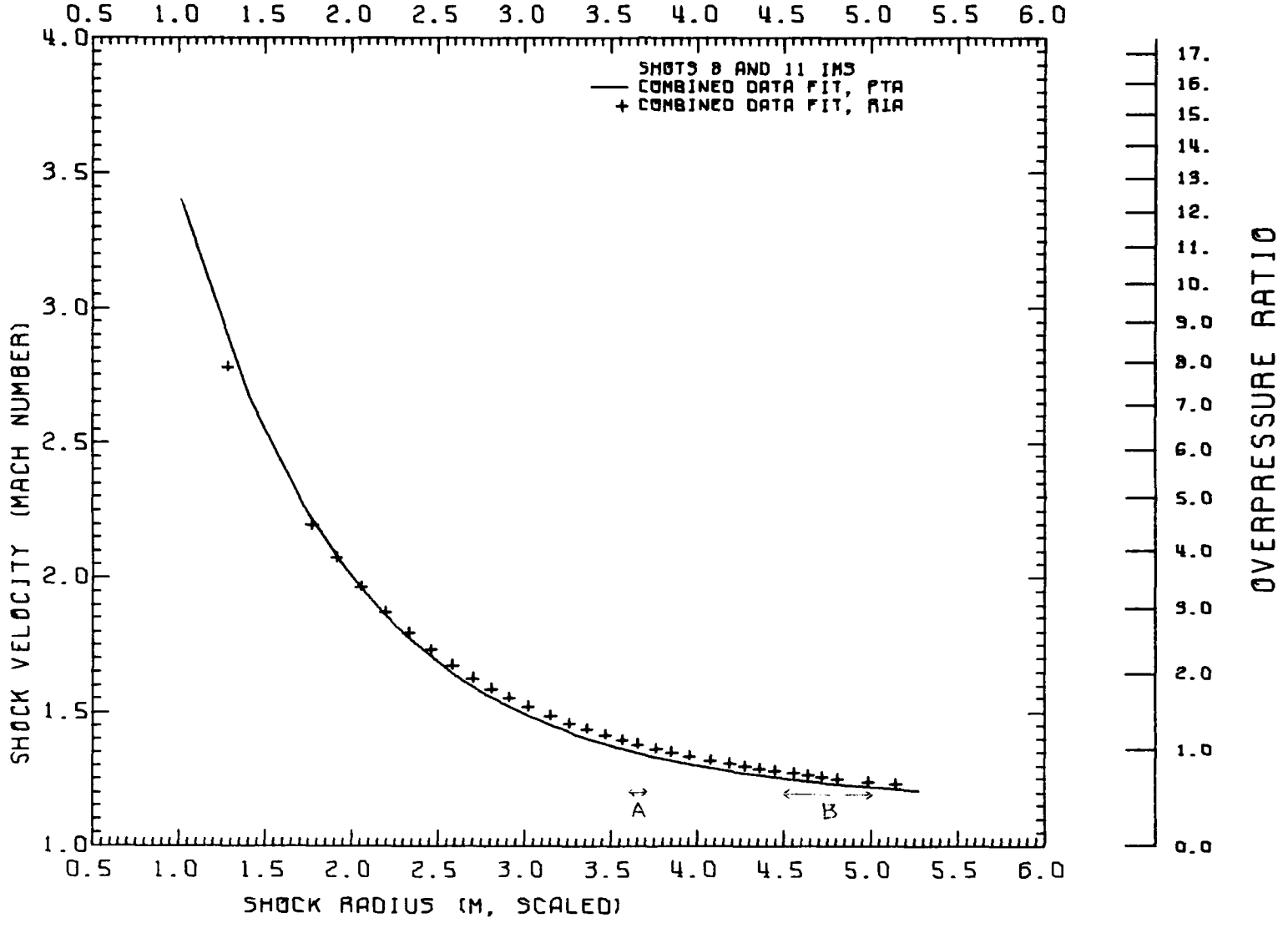

Figure 4. Interaction Mach stem strengths.

the positions of the shock front were measured at some distance above or below the interaction plane, and it was necessary to make an assumption about the shape of the Mach stem shock. The most consistent results were obtained when it was assumed that the Mach stem shocks were spherical and centered on the point where the axis joining the two charge centers intersected the interaction plane. Further study is required to justify this assumption, however.

A second uncertainty concerning the Mach stem shock data presented in Figures 3 and 4 is the distance beyond which the data measured at the interaction plane may be influenced by the ground Mach stem. The triple-point trajectory above the ground surface rises to meet the triple point coming down from the interaction plane, until the interaction Mach stem is met by the Mach stem from the ground surface. The distance where the two Mach stems meet is approximately that shown by arrow "A" in Figure 4. At distances greater than that indicated by this arrow, the interaction Mach stem and the ground Mach stem partly overlap to form a shock front which finally replaces the interaction Mach stem below the interaction plane, at a distance approximately indicated by arrow "B". Beyond the range indicated by arrow "B", the Mach stem above the interaction plane is increasingly modified in this manner.

Results similar to those plotted in Figures 3 and 4 are plotted in Figures 5 and 6 for the Mach stem shocks above and below the interaction plane for Shots 9 and 10. Shot 9 RIA trajectory data for the Mach stem below the interaction plane were not included with the Shot 10 RIA data because of a slight but significant displacement in time relative to the Shot 10 data, probably due to a small error in establishing time zero for one of the experiments (RIA only). Such a difference in radius-time data does not affect strength-versus-radius results if the different radius-time data are not combined.

The radii at which the interaction Mach stems become affected by the ground Mach stem (as explained above) are marked in Figure 6 by arrows "A" and "B".

The particle trajectory analysis curves from Figures 2, 4 and 6 have been plotted together in Figure 7 to provide a comparison of the Mach stem shock strengths for the two heights of burst. Another comparison is shown in Figure 8, in terms of reflection factors determined by calculating the cubes of the ratios of the radii at which the Mach stem shock and primary shock were of the same strength. These results are plotted versus the radius of the Mach stem measured

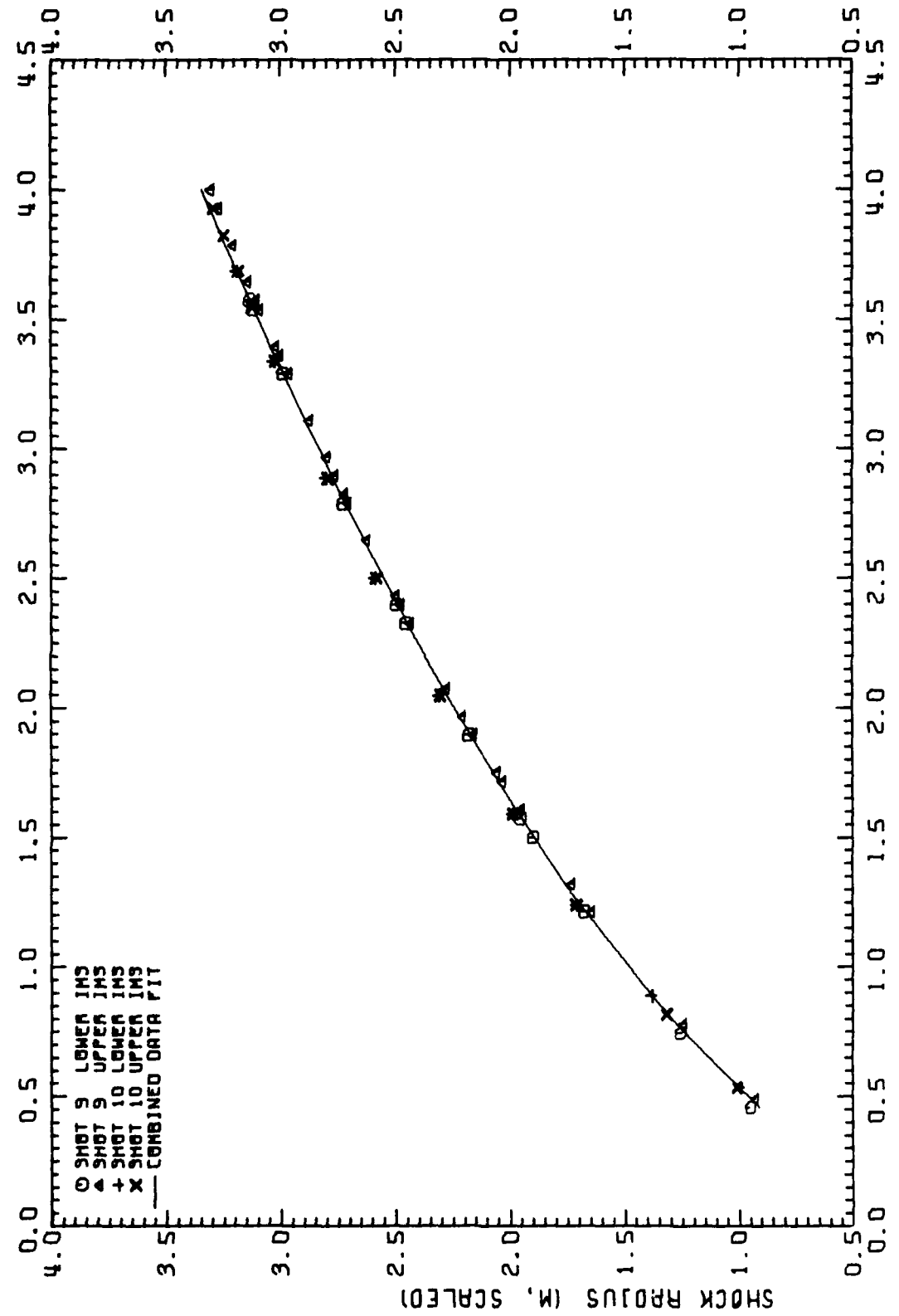

Figure 5. Interaction Mach stem trajectories.

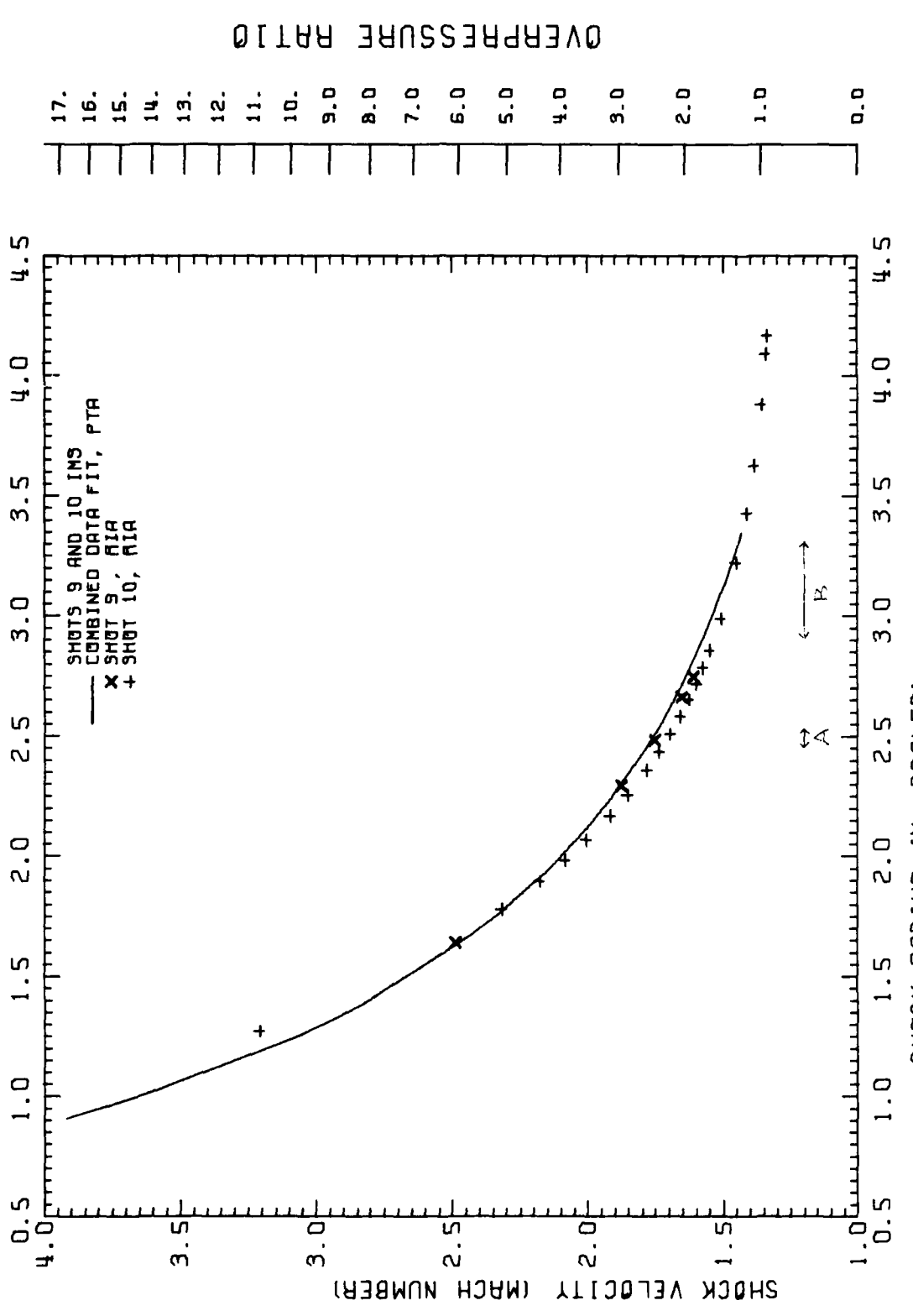

Figure 6. Interaction Mach stem trajectories.

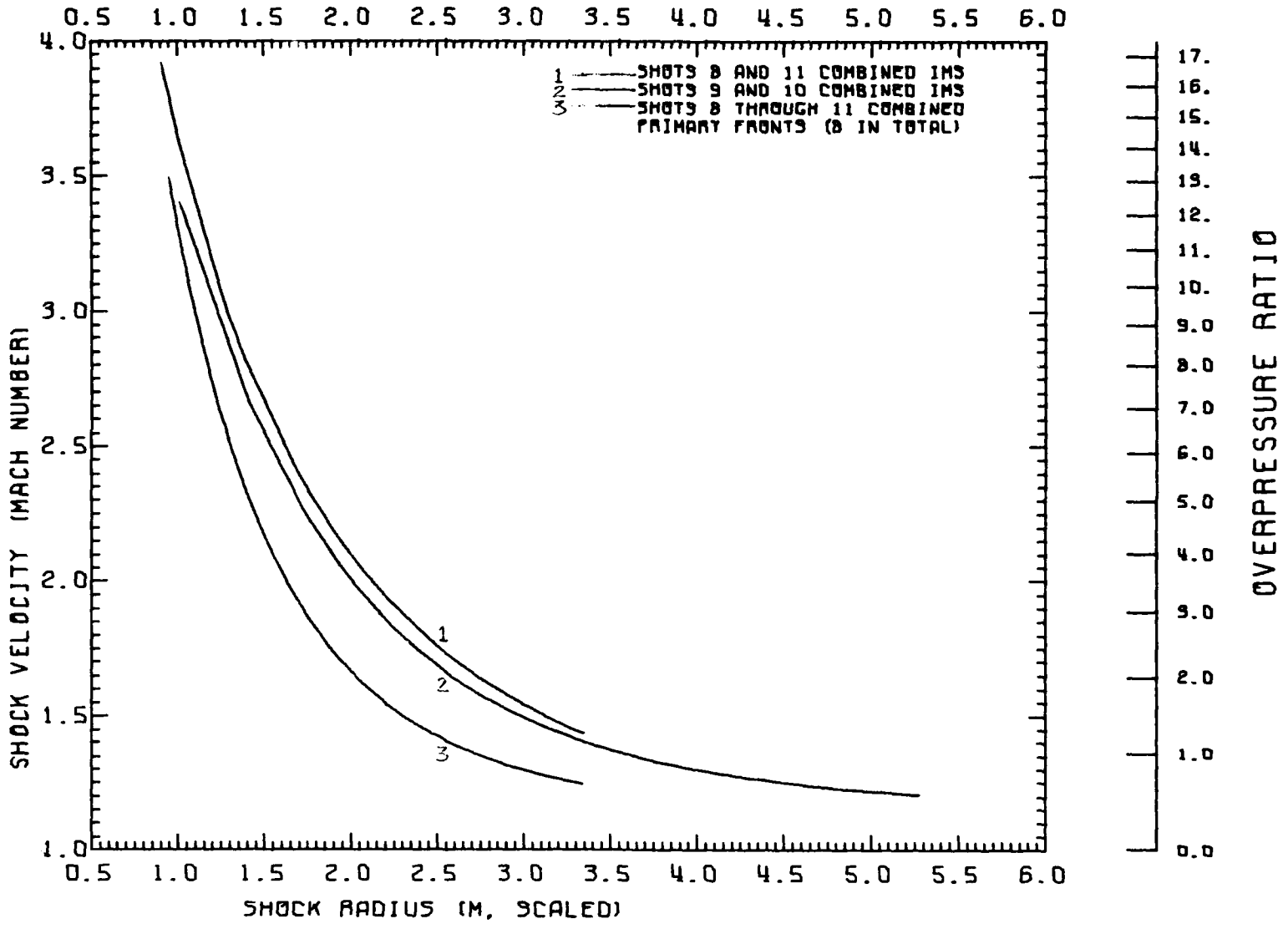

Figure 7. Interaction Mach stem strengths.

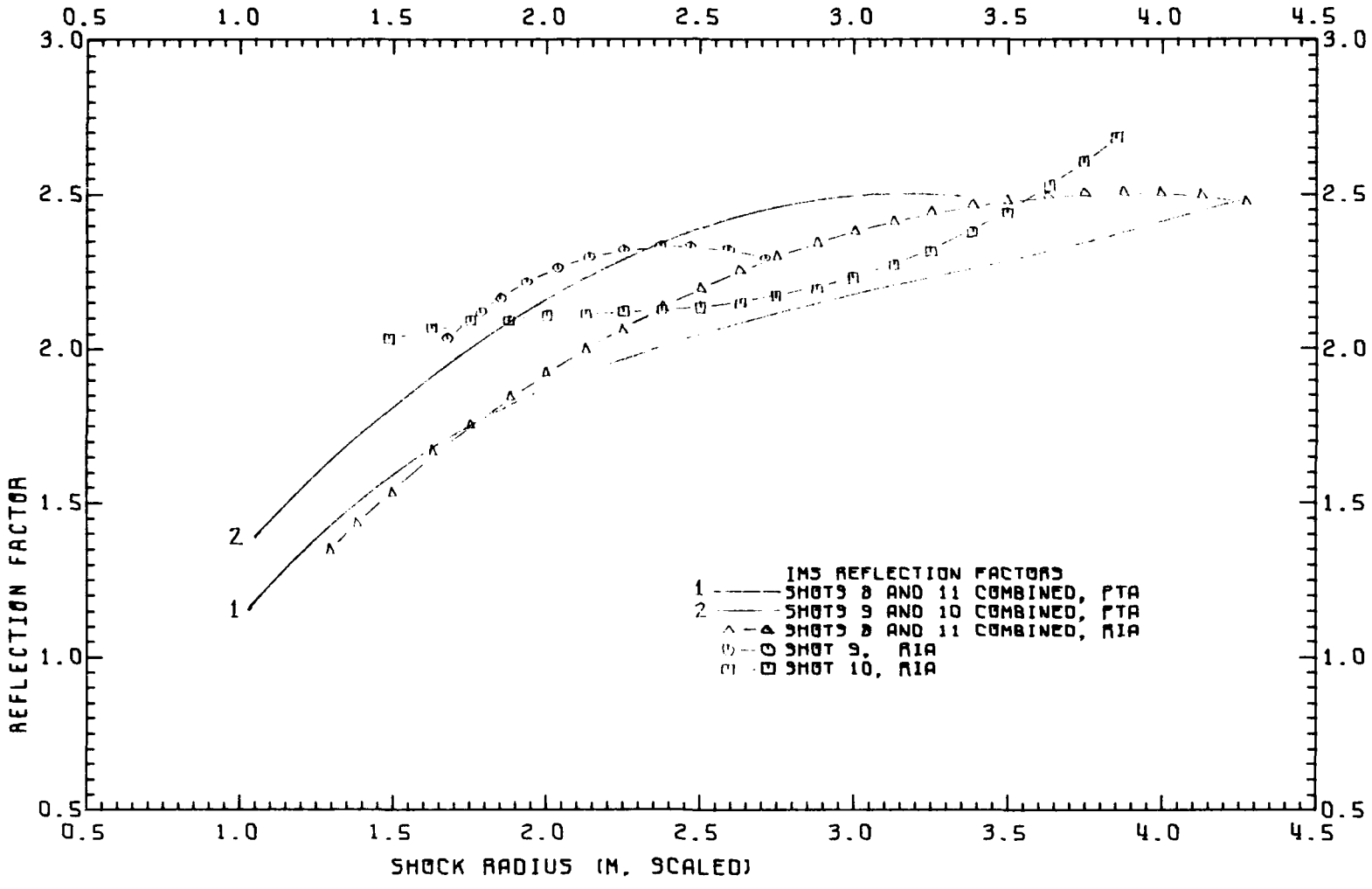

Figure 8. Interaction Mach stem strengths.

from the point where the axis joining the two charge centers intersects the interaction plane, i.e., the horizontal distance along the interaction plane. (Mach stem reflection factors computed by some authors have been plotted against the oblique radius from the charge center to the point where the Mach stem intersects the ground.)

Reflection factors computed using the refractive image analysis results are also shown in Figure 8. While there is some agreement between the results of the methods of analysis for Shots 8 and 11 and Shot 9, the RIA results for Shot 10 appear to be unusual. It should be pointed out again that all RIA results were computed from measurements made very close to the reflecting plane, whereas the PTA measurements were extended above and below the plane.

2-3 MACH STEM SHOCKS ABOVE THE GROUND

The dipole experiments were designed, in part, to compare the reflection of spherical blast waves by real and ideal surfaces. The charge configurations were such that reflection of the primary wave from the lower charge at the interaction plane was accompanied by a reflection of the same wave from the ground surface.

The RIA results (Dewey, et al, 1975), which were obtained by making measurements about 0.5 m above the ground, showed the Mach stem shocks over rough ground (Shots 10 and 11) to be significantly weaker than the Mach shocks at the interaction plane at the same radial distance. The shocks over the smooth ground (Shots 8 and 9) were also weaker than the interaction shocks, but to a much smaller extent.

The Mach stem shock strengths for Shots 8 and 11, obtained from the smoke puff movements, are illustrated in Figure 9 but do not show the differences observed using the refractive image analysis. Undoubtedly, this is due to the fact that the shock front arrivals at the smoke puffs were measured throughout the Mach stem regions at distances up to 7.5 m from the reflecting surfaces. The results shown in Figure 9, therefore, indicate that the differences in Mach-stem shock strength are extremely height-dependent, as might be expected. (A variation of shock front strength with height above the ground surface implies a deviation of the shape of the shock front from the spherical shape that has been assumed in these calculations. The authors believe this problem justifies further study.)

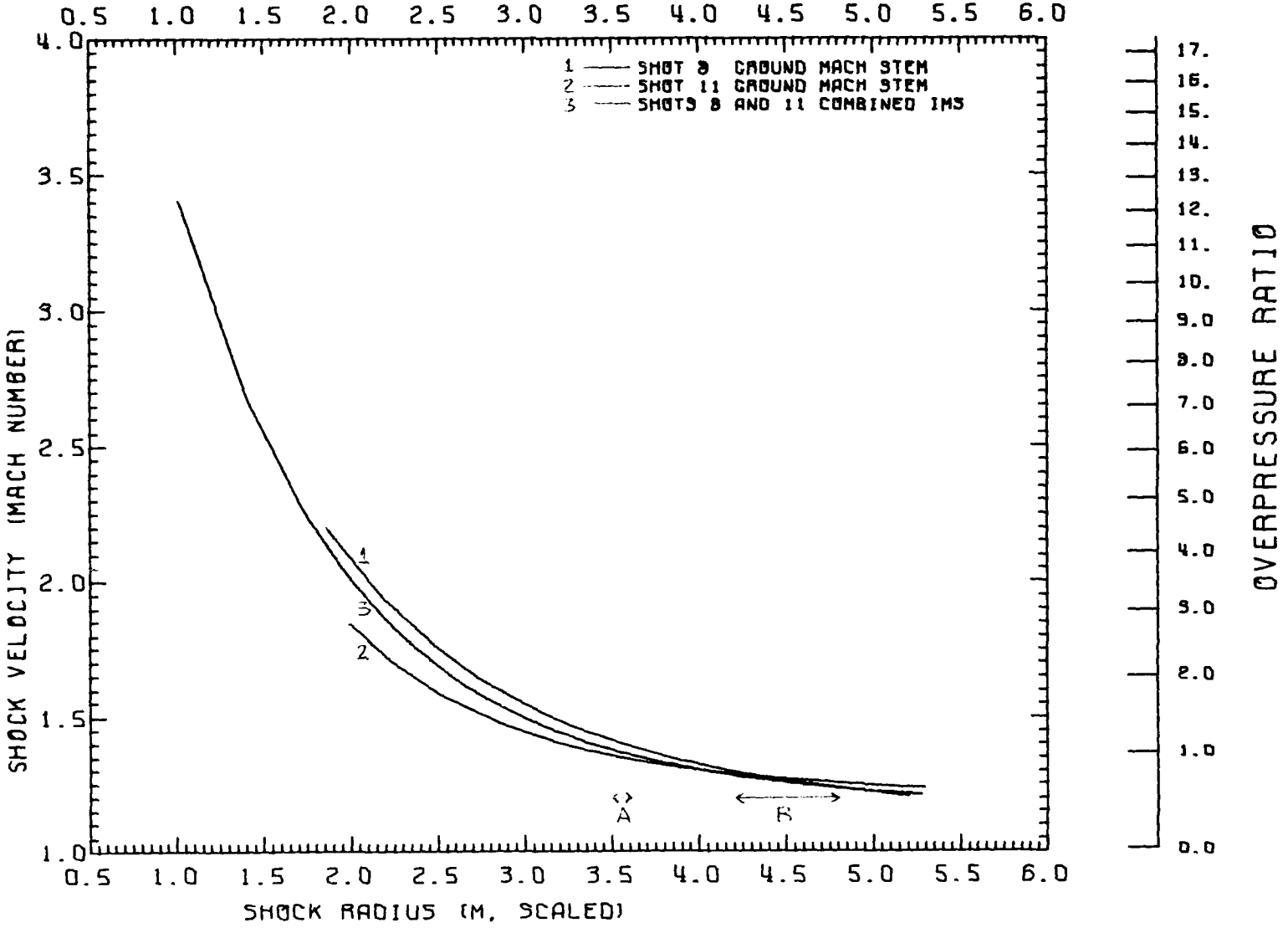

Figure 9. Ground Mach stem strengths.

The arrow labeled "A" in Figure 9 marks the approximate distance at which the interaction Mach stem first begins to influence the ground Mach stem, in a manner described in the preceding section, and the arrow "B" indicates a range in which this influence becomes complete. Beyond the distances indicated by the second arrow, the shock which was first reflected below the interaction plane, and then re-reflected by the ground surface, has overtaken the original ground Mach stem, possibly reinforcing it.

The ground Mach stem results for Shots 9 and 10 were found to be similar to those shown in Figure 9 for Shots 8 and 11.

SECTION 3

COMPARISON OF BLAST WAVE PROFILES

3-1 PARTICLE VELOCITY TIME-HISTORIES.

In the first four volumes of this series, time-histories of particle velocity, density, hydrostatic overpressure and dynamic pressure were presented for a number of fixed locations within the region of the smoke puff array. Of all the physical properties derived from the high-speed photography of the smoke puffs, the particle velocity within the blast waves is undoubtedly the most accurately measured. Figure 10 shows the time variation of particle velocity calculated at four horizontal radii within the ideal Mach stem (IMS) regions for Shots 8 and 11. The curves for the two experiments for positions at equal distances above and below the interaction plane and at the same radial distance from the axis joining the two charge centers are plotted together.

For each radial distance, the four curves are very similar, except at the extreme right-hand side of the curves, where the curves for locations above and below the interaction plane show differences which are probably significant, particularly at scaled radial distances of 4 m and 5 m. This is due to lack of symmetry in the dipole experiment at later times, a matter which will be discussed later in this report. Because of the similarity of the four curves at each radial distance, it is appropriate to trace a single curve within the family in order to simplify further comparisons. For example, the four curves showing the variation of particle velocity at a radial distance of 4 m are replotted as Figure 11, together with a single curve drawn to represent the family, and "error" bars to show the range of values being represented by the single curve.

Similar results were obtained for Shots 9 and 10 at three radial positions, with even closer agreement between the curves from the two shots.

The median curves for Shots 8 and 11 are plotted with the corresponding curves for Shots 9 and 10 for radial distances of 2.5 and 3 m in Figure 12A. In this figure, the curves are plotted against real time, the time elapsed after the detonation of the charges. In Figure 12B, the curves for the same two radial distances have been shifted in time to a common time of shock arrival. As can be

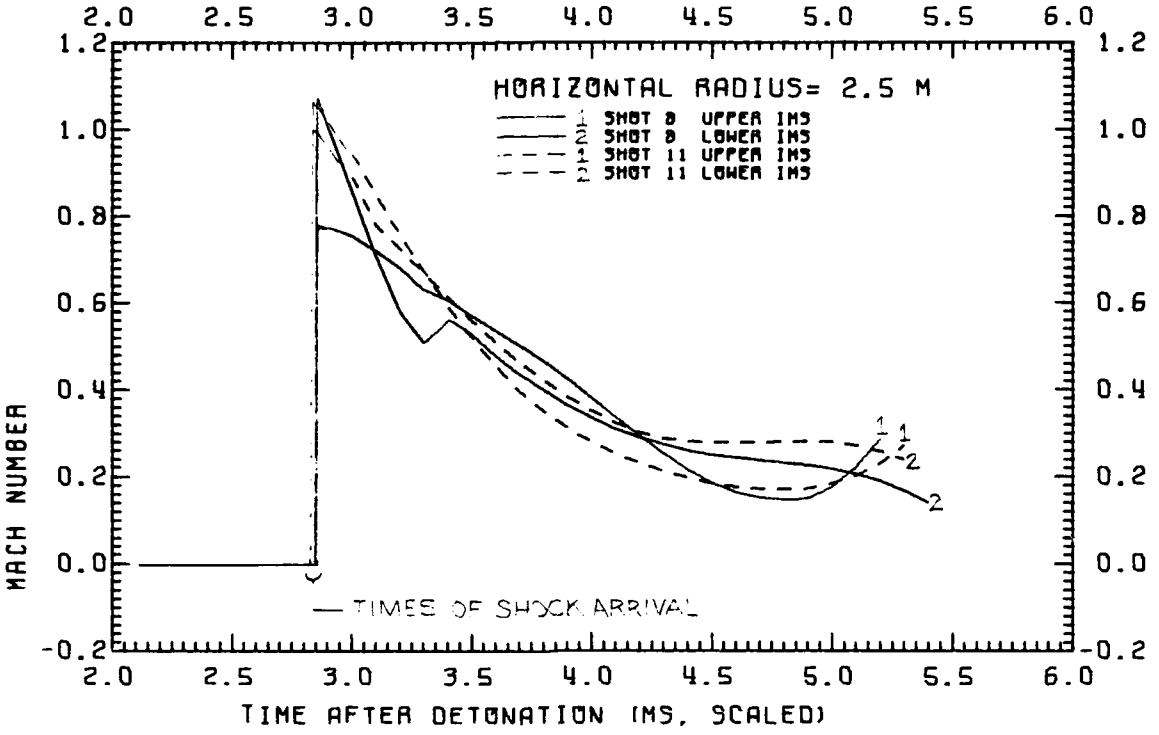

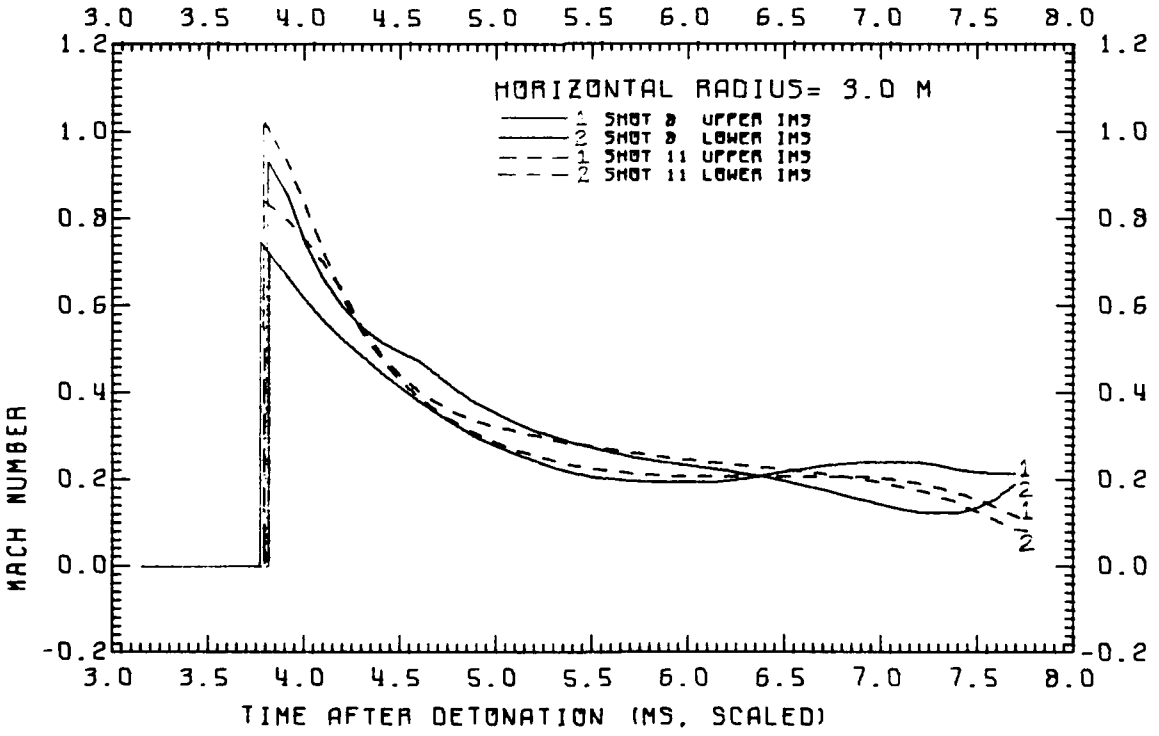

Figure 10A. Particle velocity time-histories.

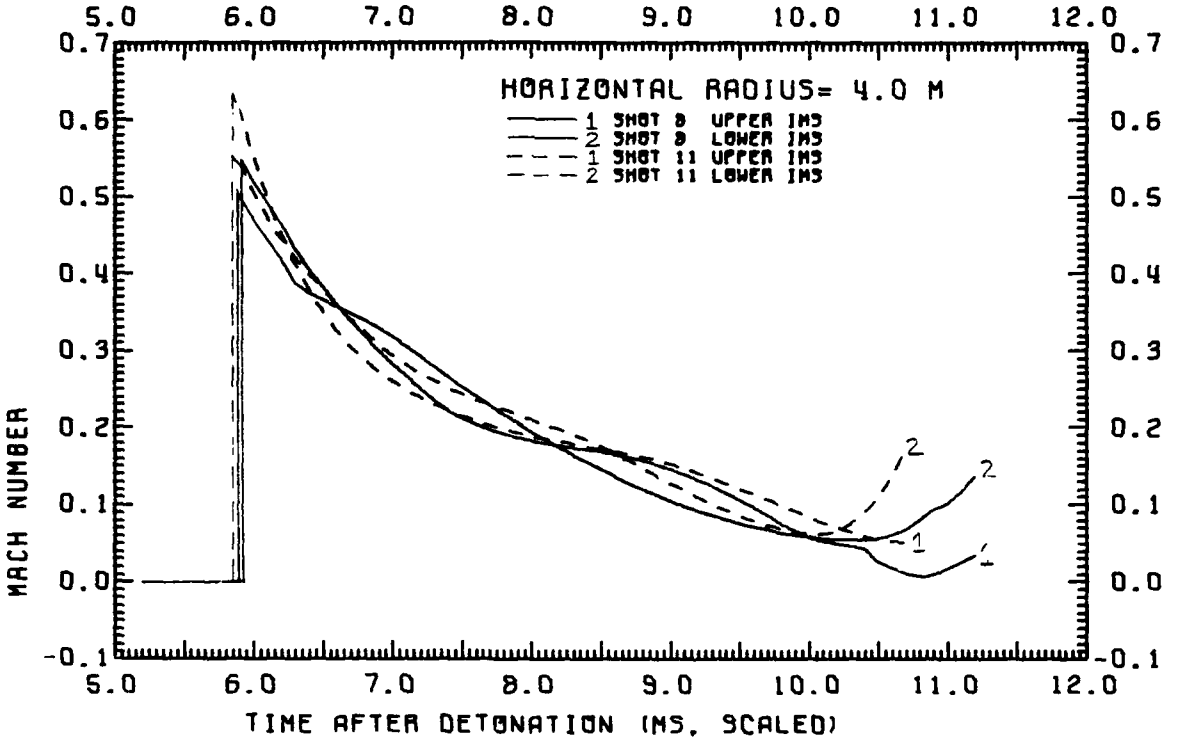

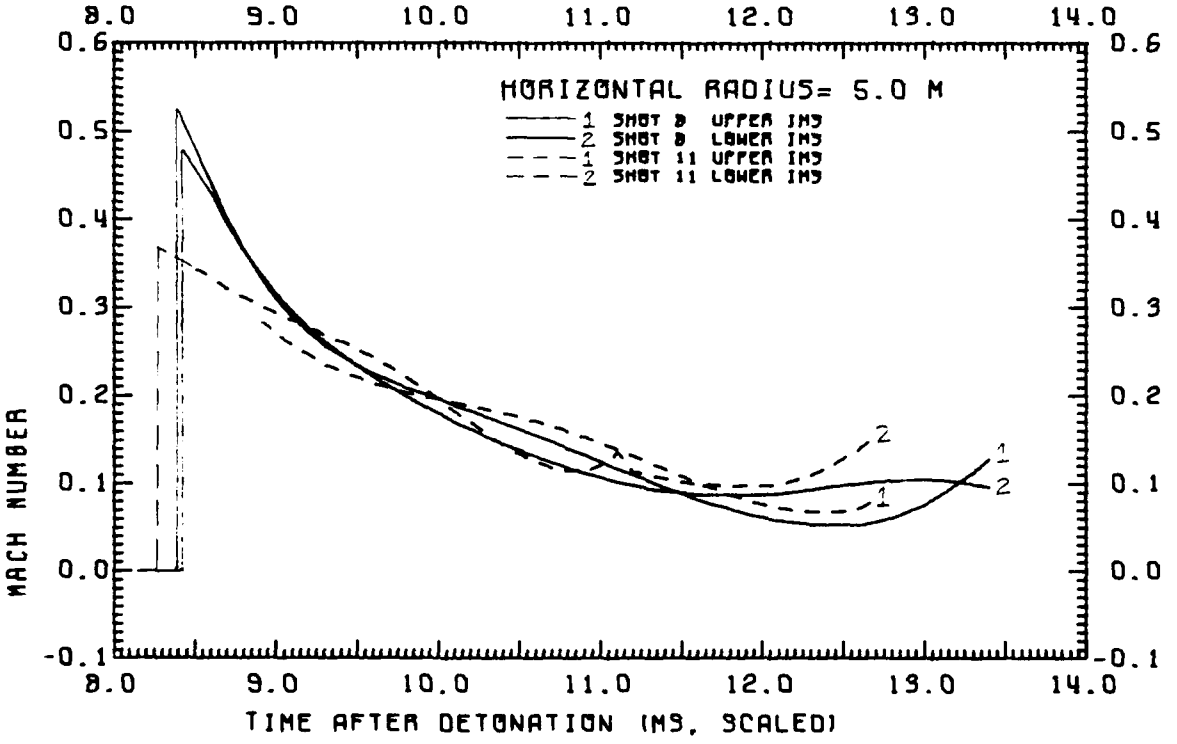

Figure 10B. Particle velocity time-histories.

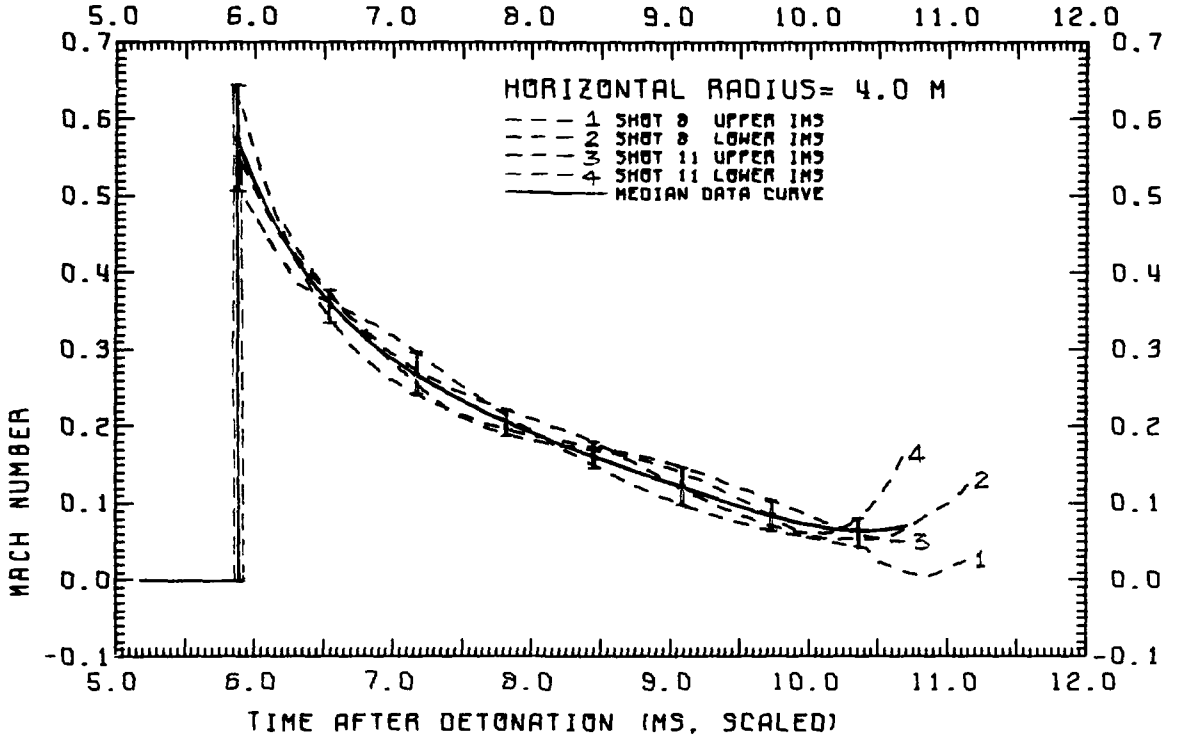

Figure 11. Method of averaging time-histories.

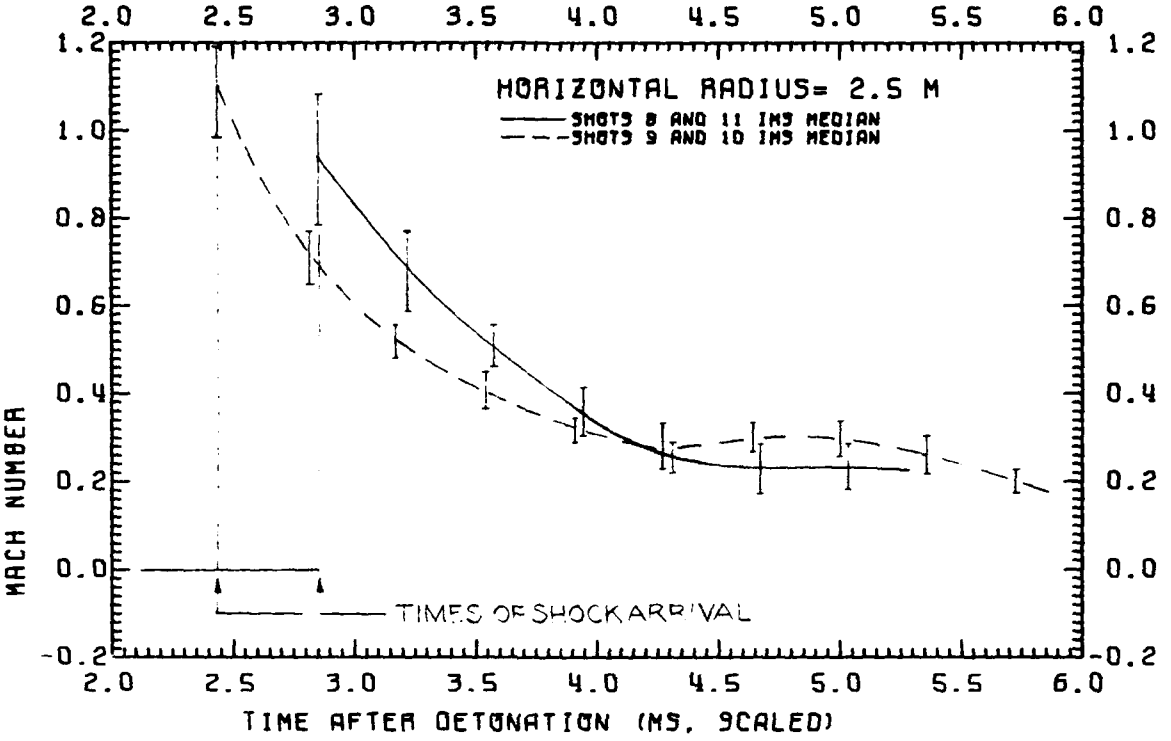

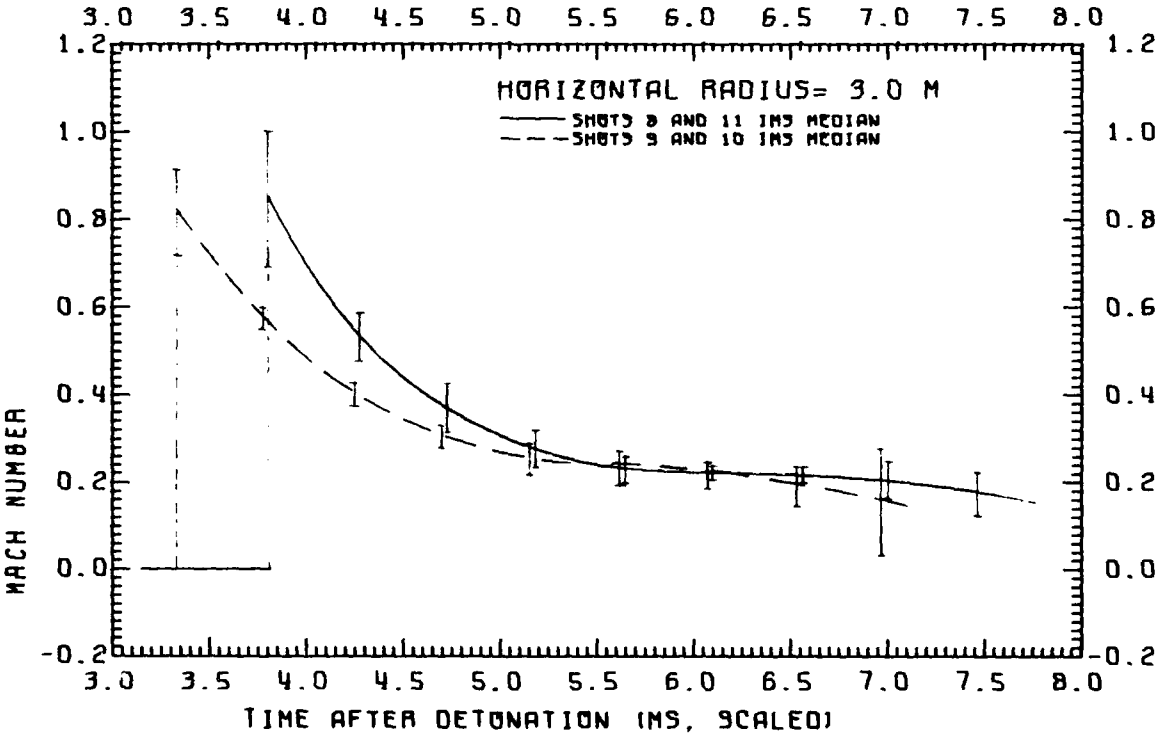

Figure 12A. Particle velocity time-histories.

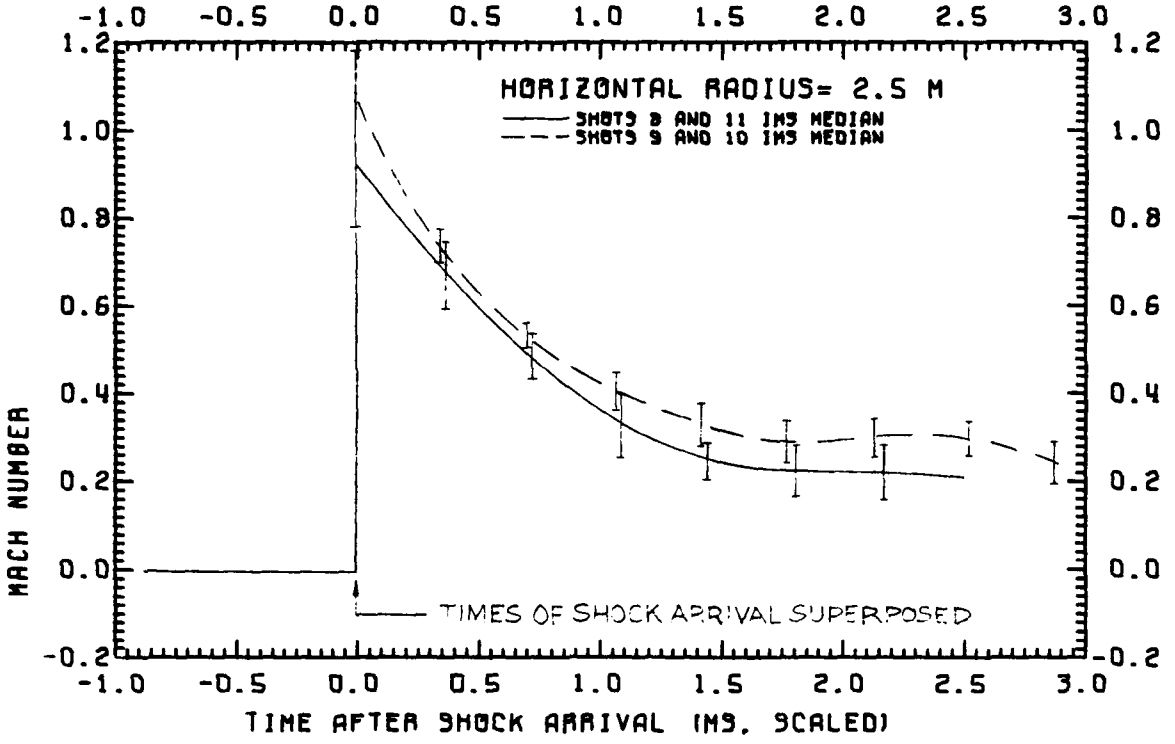

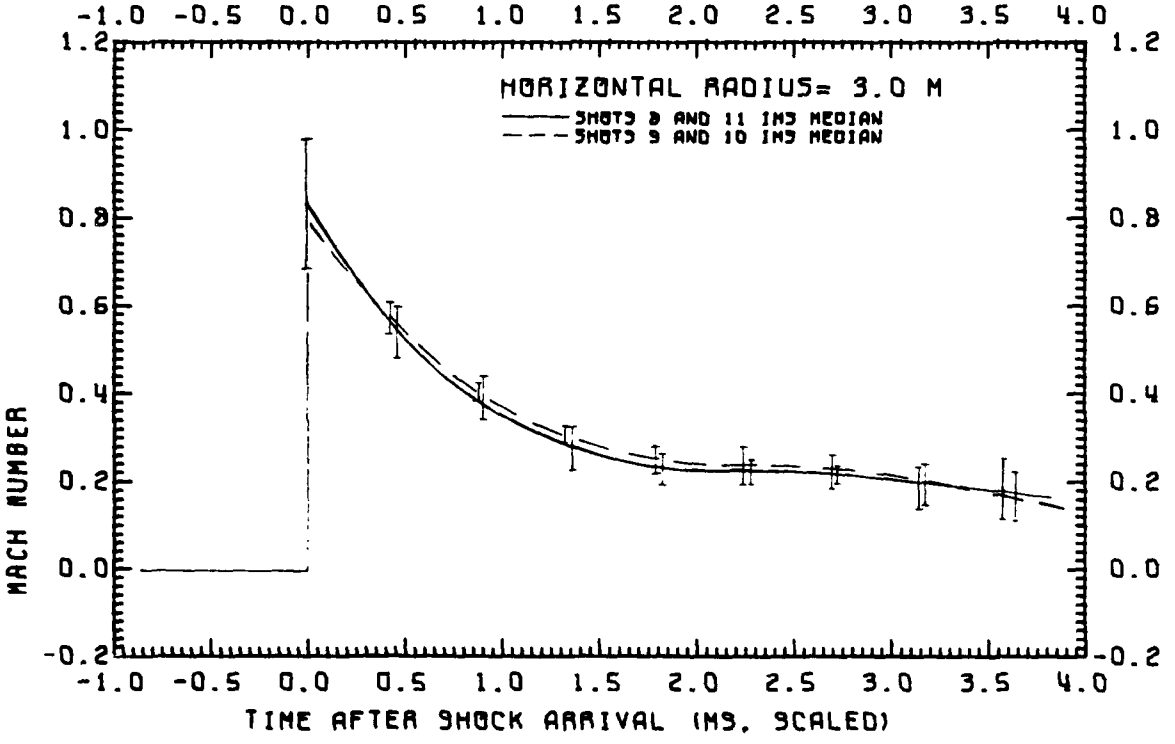

Figure 12B. Particle velocity time-histories.

seen, the curves for the two heights of burst are identical to the extent that their ranges of uncertainty overlap.

In Figure 13, the median curves representing the particle velocity time-histories at the four radial positions in the IMS region have been plotted together with time-histories at the same radial distances in the region of the Mach stem above the ground surface. In each case, while the particle velocity immediately behind the ground Mach stem shock is sometimes lower than for the interaction Mach stem, the particle velocity in the ground Mach stem at later times becomes greater than that in the interaction Mach stem. This is a consistent pattern which will be further demonstrated for the other physical parameters described below.

3-2 HYDROSTATIC OVERPRESSURE TIME-HISTORIES.

The hydrostatic overpressure time-histories at four radial distances in the Mach stem waves for Shots 8 and 11 are shown in Figure 14. Shown are the median curves drawn between the four results above and below the interaction plane for the two experiments, together with curves for points at the same radial distance but in the Mach stem above the ground surface (the GMS region).

It will be recalled that hydrostatic overpressure is obtained from the photographically measured particle trajectories by first determining the density of each gas element defined by four smoke puffs and then applying an equation of state to that gas element based on the entropy change introduced by the passage of the first shock front to traverse the element. As pointed out in the previous volumes, the determination of hydrostatic overpressure is therefore not as accurate as the determination of particle velocity, and this is demonstrated in Figure 14 by the longer error bars representing the scatter of the results from the four positions. Despite the greater uncertainties, the relative shapes of the profiles for the interaction and ground Mach stems are similar to those for particle velocity, which is to say that at later times in the profile, the hydrostatic overpressure in the ground Mach stem appears to be higher than that for the Mach stem at the interaction plane. This confirms the observation of Dewey et al (1975), based on pressure profiles determined from electronic transducers which indicated that in all experiments, although the shock front pressure in the Mach stem above the ground was less

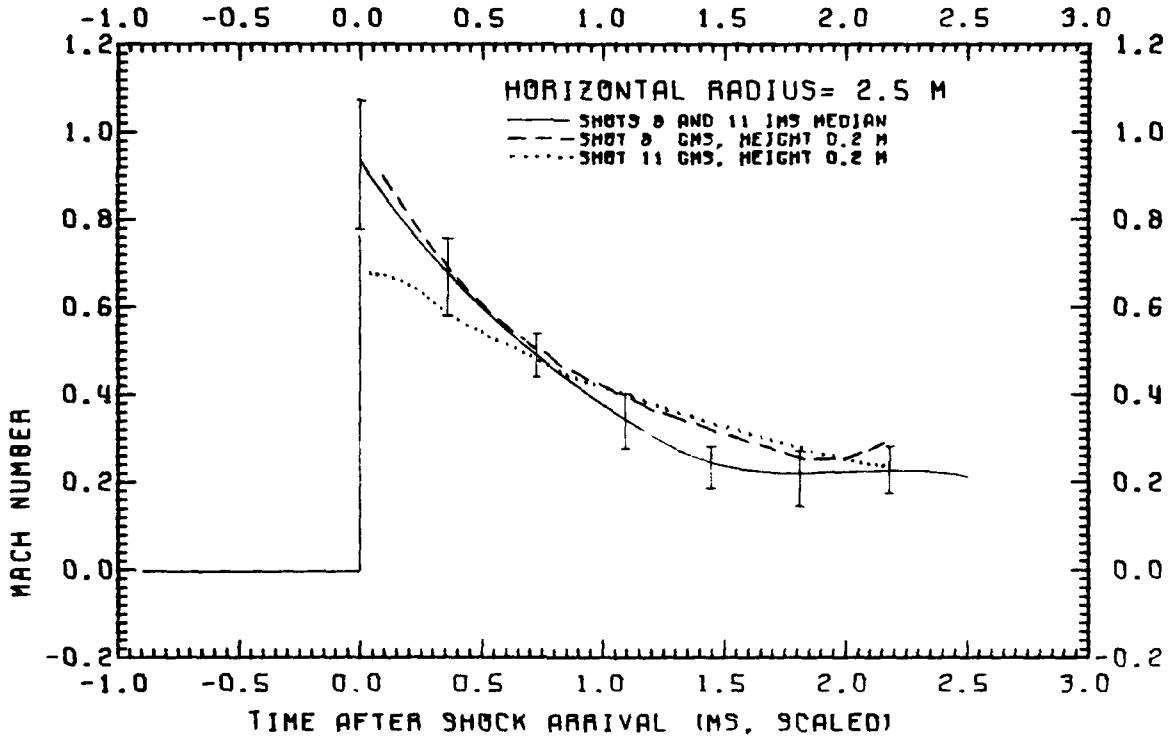

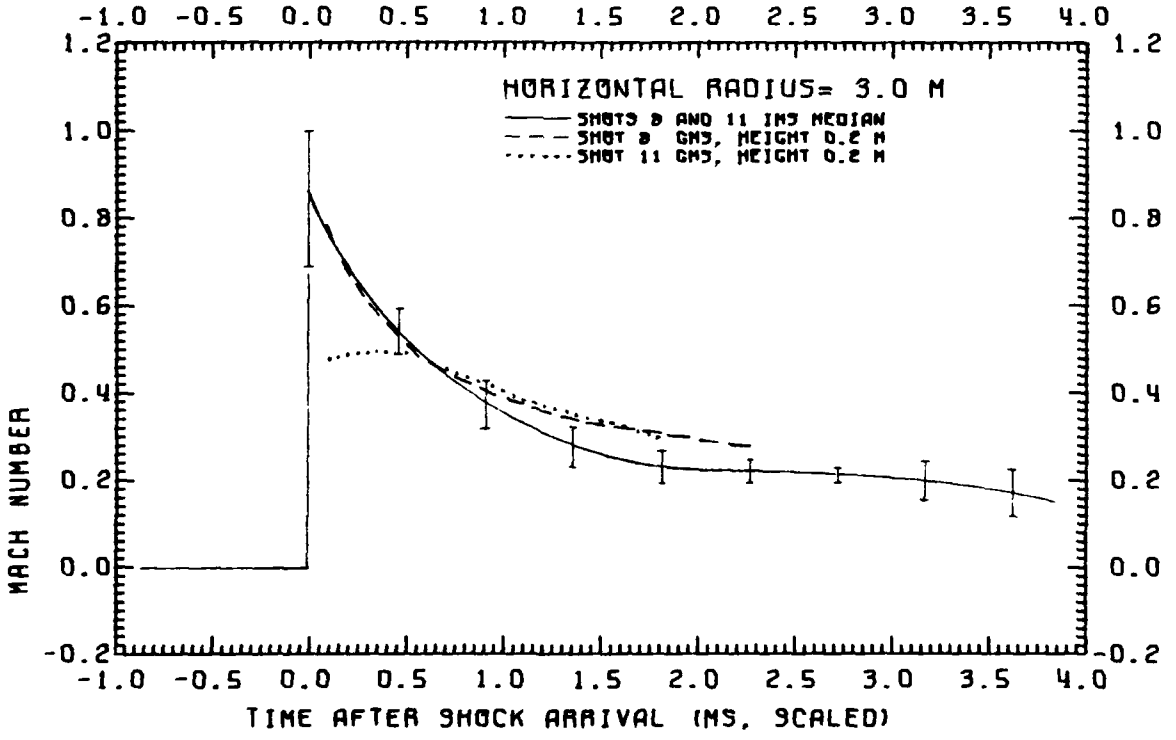

Figure 13A. Particle velocity time-histories.

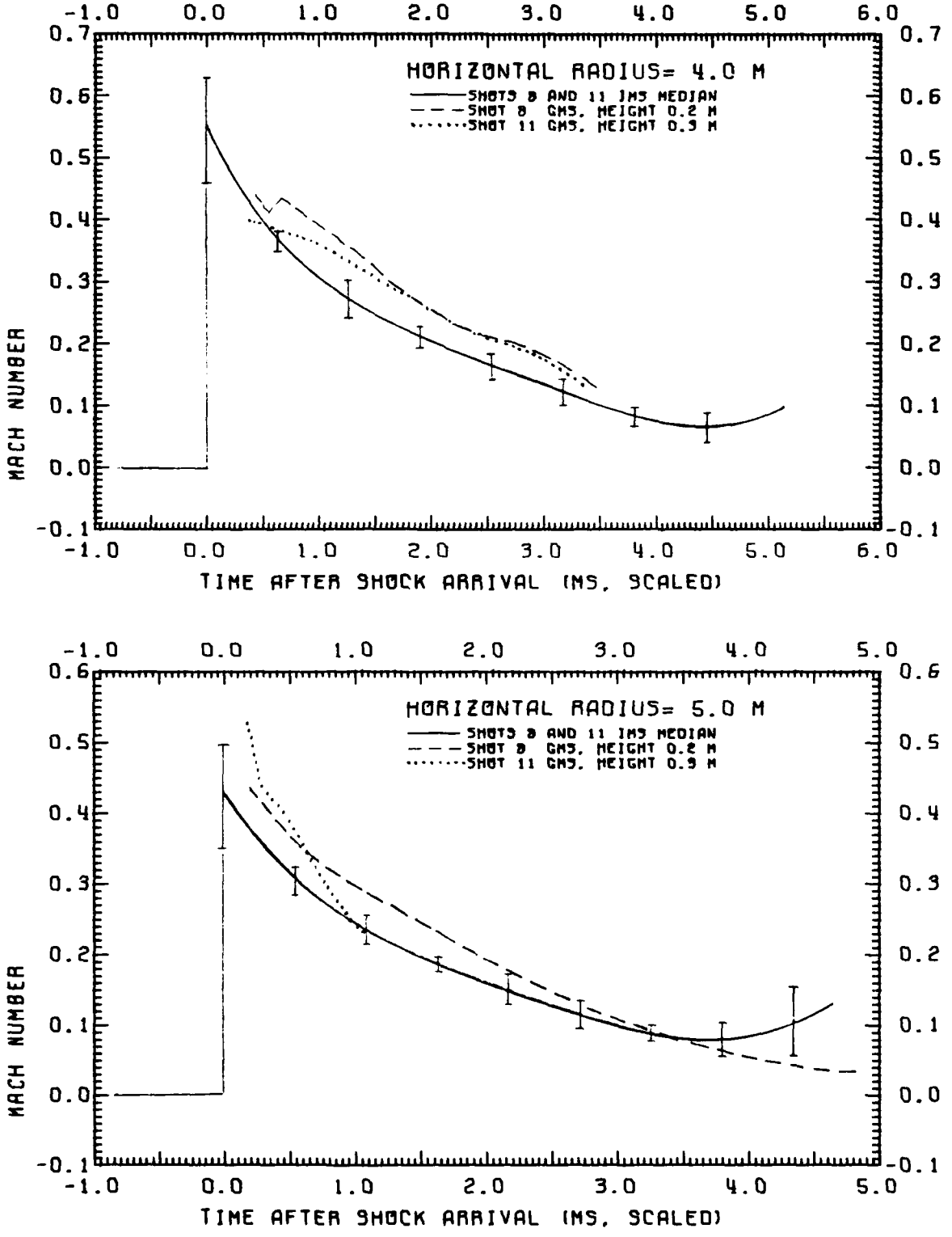

Figure 13B. Particle velocity time-histories.

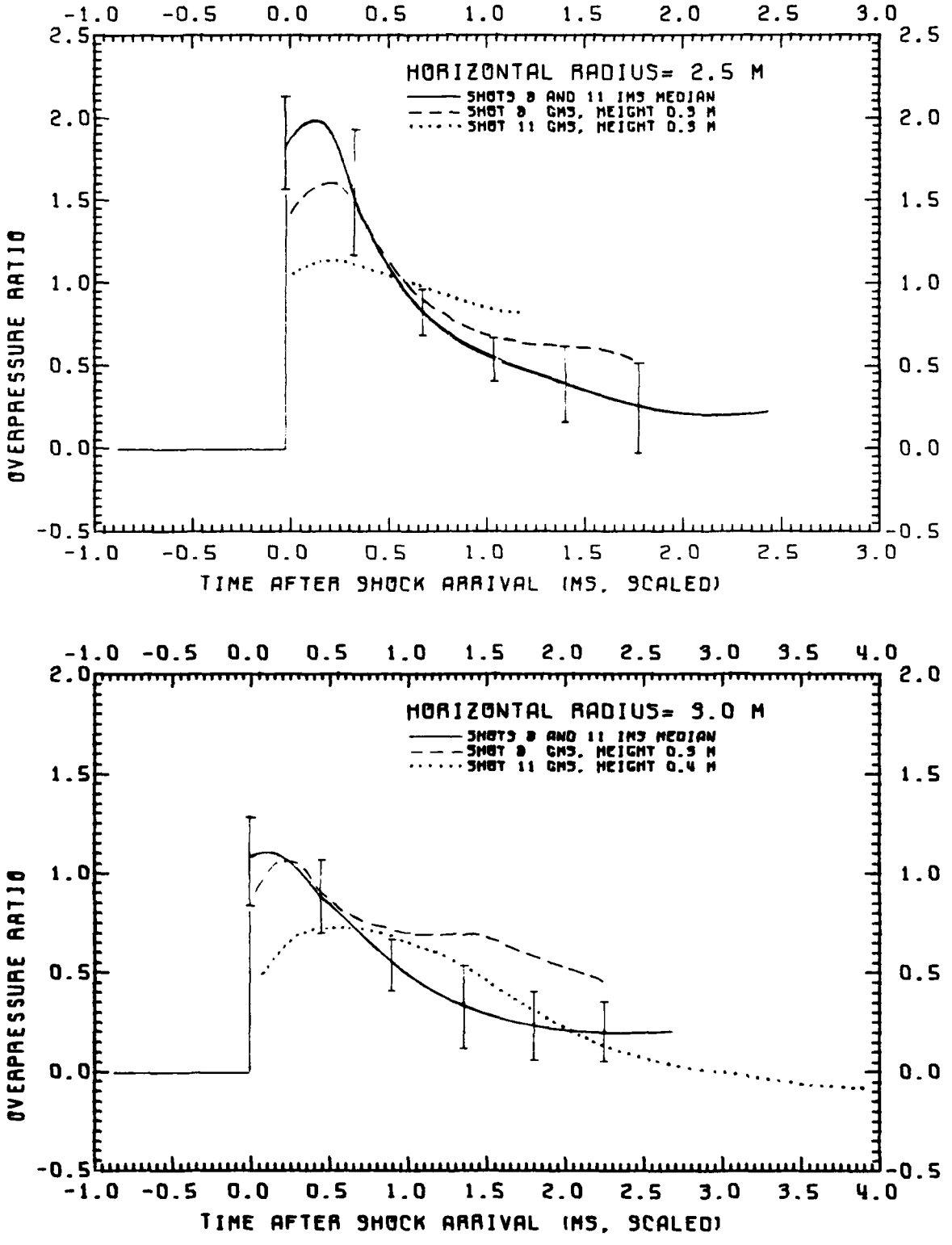

Figure 14A. Hydrostatic overpressure time-histories.

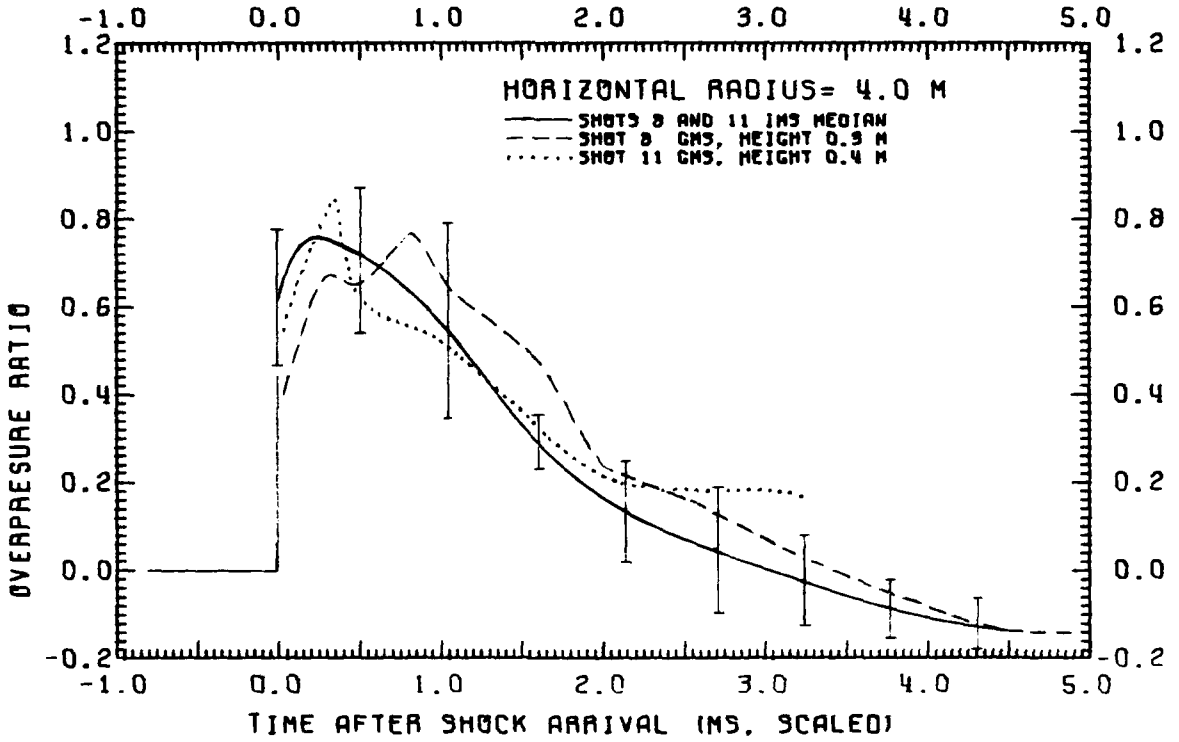

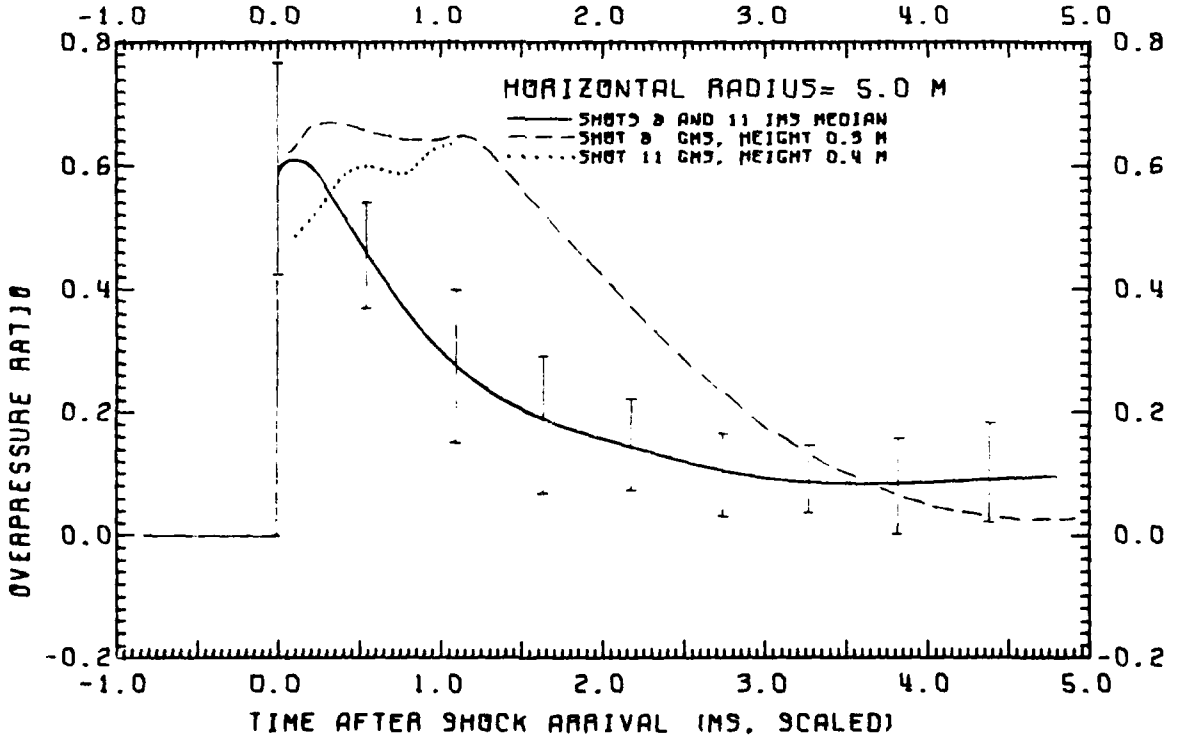

Figure 14B. Hydrostatic overpressure time-histories.

than that at the same radial distance in the Mach stem at the interaction plane, the pressure impulses were consistently greater above the ground.

Similar results are shown in Figure 15 for Shots 9 and 10 at two radial distances.

3-3 DYNAMIC PRESSURE TIME-HISTORIES.

Dynamic pressure time-histories are shown for Shots 8 and 11 in Figure 16, and for Shots 9 and 10 in Figure 17. Shown are curves with the error bars representing the medians of four curves from the Mach stems above and below the interaction plane, and curves for the same radial distances in the ground Mach stems. Again, the consistent pattern is seen of higher values of dynamic pressure in the shock wave above the ground at later times compared to those at the interaction plane.

Care must be taken in drawing conclusions from the above results. In particular, it should not be concluded at this time that the extended duration of the time-histories in the Mach stem above the ground surface is due to the difference between a reflection from a real surface compared with a reflection from an ideal surface. The observed differences may be associated with a lack of symmetry in the dipole experiments. This is illustrated in Figure 18, which is a generalized impression of the shock patterns which might be expected from the dipole explosions, with charges spaced as for Shots 8 and 11. Consider the two reflected shocks between the upper and lower triple-point trajectories for the lower charge. These shocks intersect along a horizontal line through the lower charge. After passing the intersection point of the triple-point trajectories "A", the reflected shocks will continue onward, and the downward-facing reflected shock will again reflect from the ground surface and might eventually be expected to form a second Mach stem, starting at "B", as shown in Figure 18.

However, a corresponding reflection cannot occur at the interaction plane for the original upward-facing reflected shock. Such a re-reflection would require a matching shock, approaching from above the interaction plane, and one does not exist. The radial distances at which time-history profiles were shown in Figures 10 through 17 (for Shots 8 and 11) are marked in Figure 18, and it can be seen that, especially at the 5 m radial positions, differences might be expected in the profiles of the Mach stem waves above the ground and

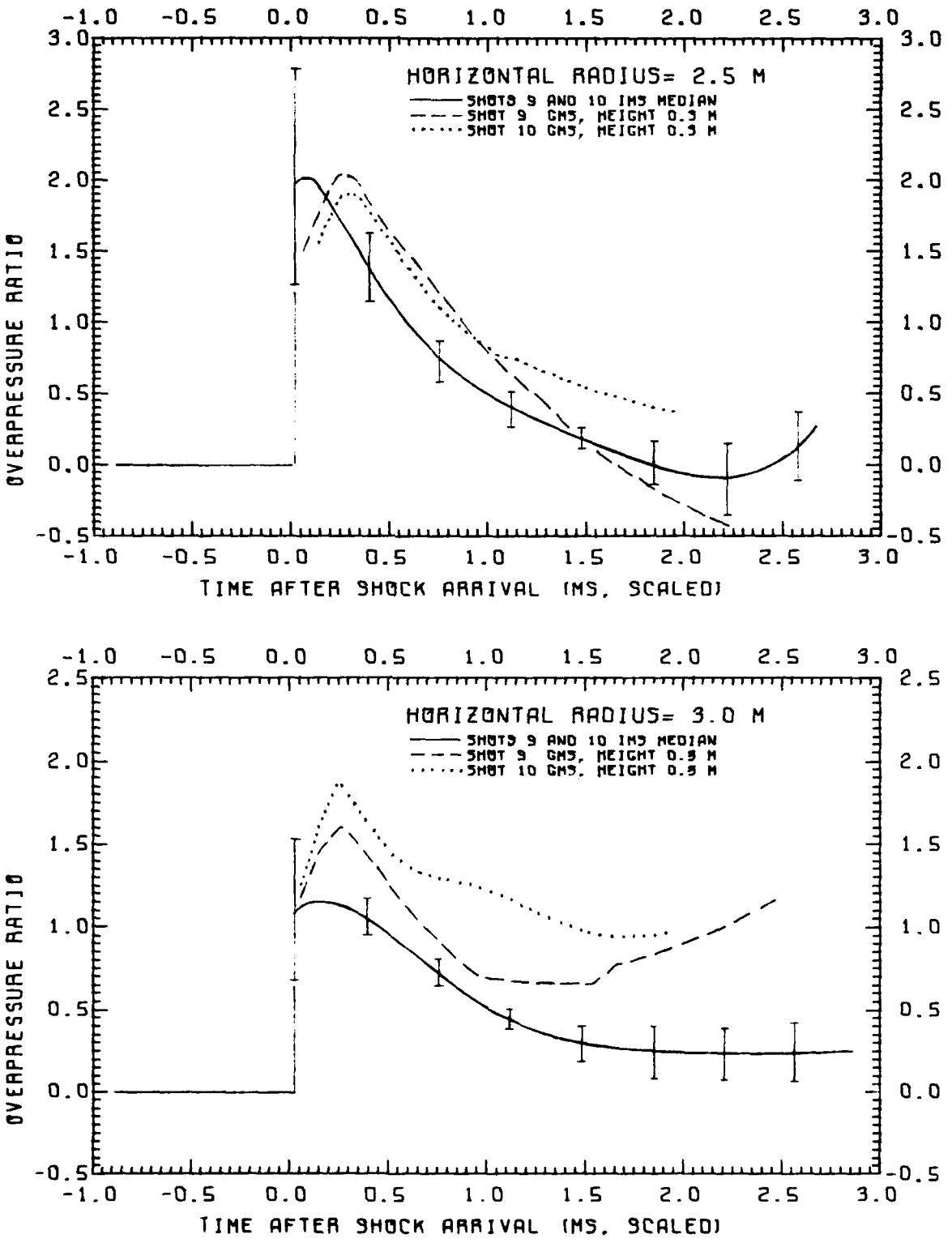

Figure 15. Hydrostatic overpressure time-histories.

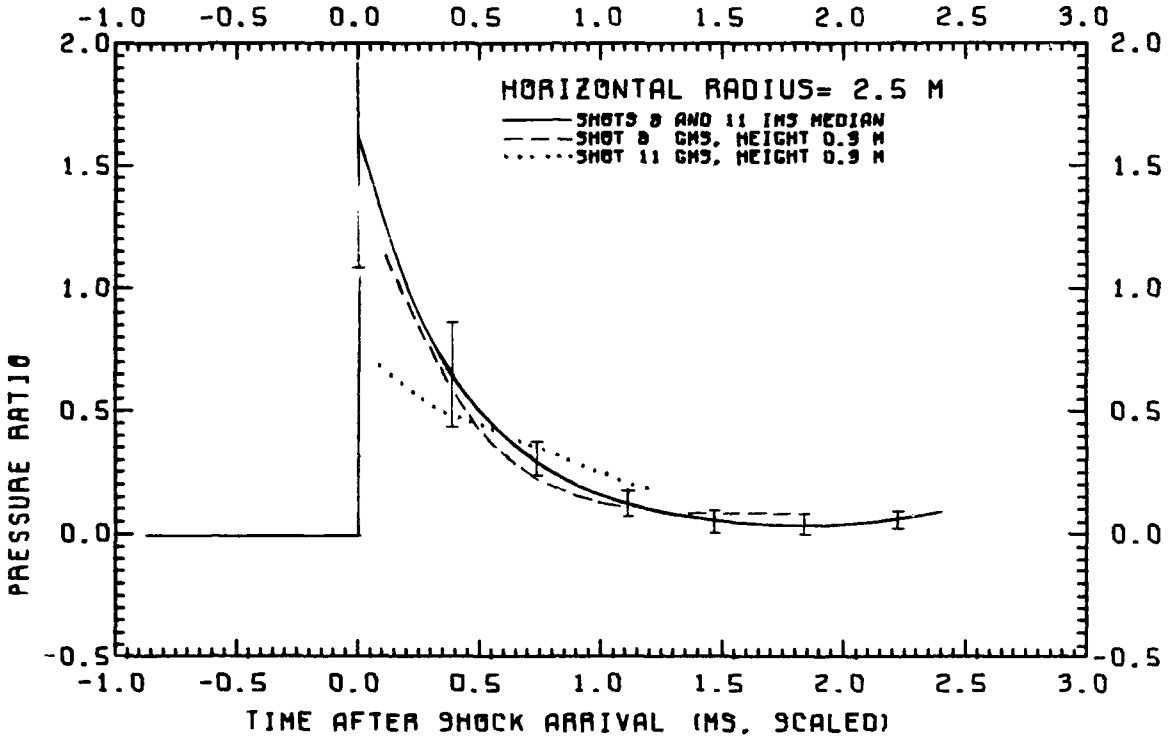

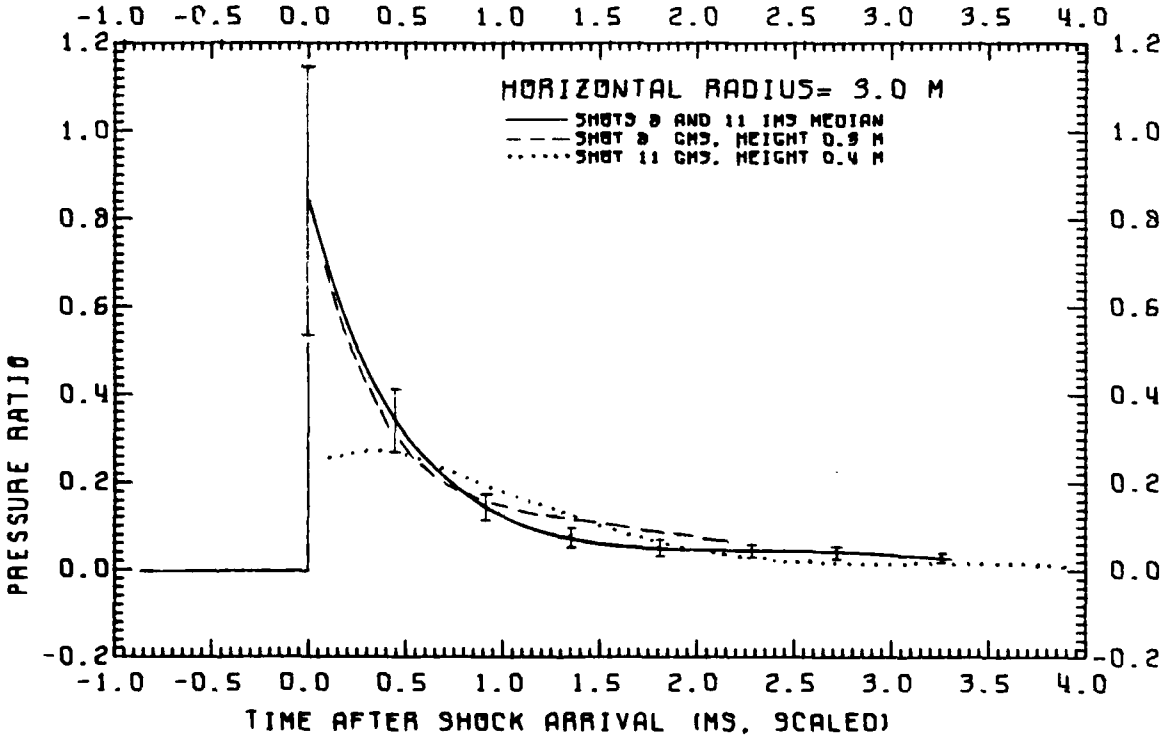

Figure 16A. Dynamic pressure time-histories.

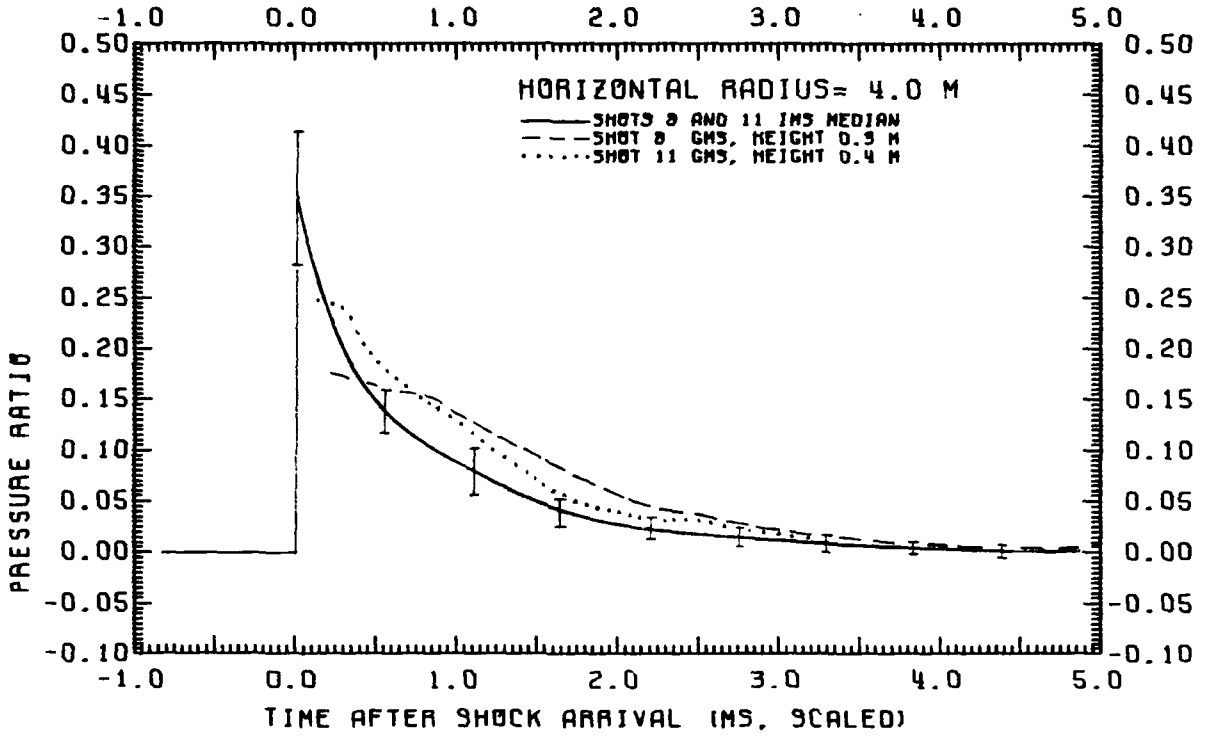

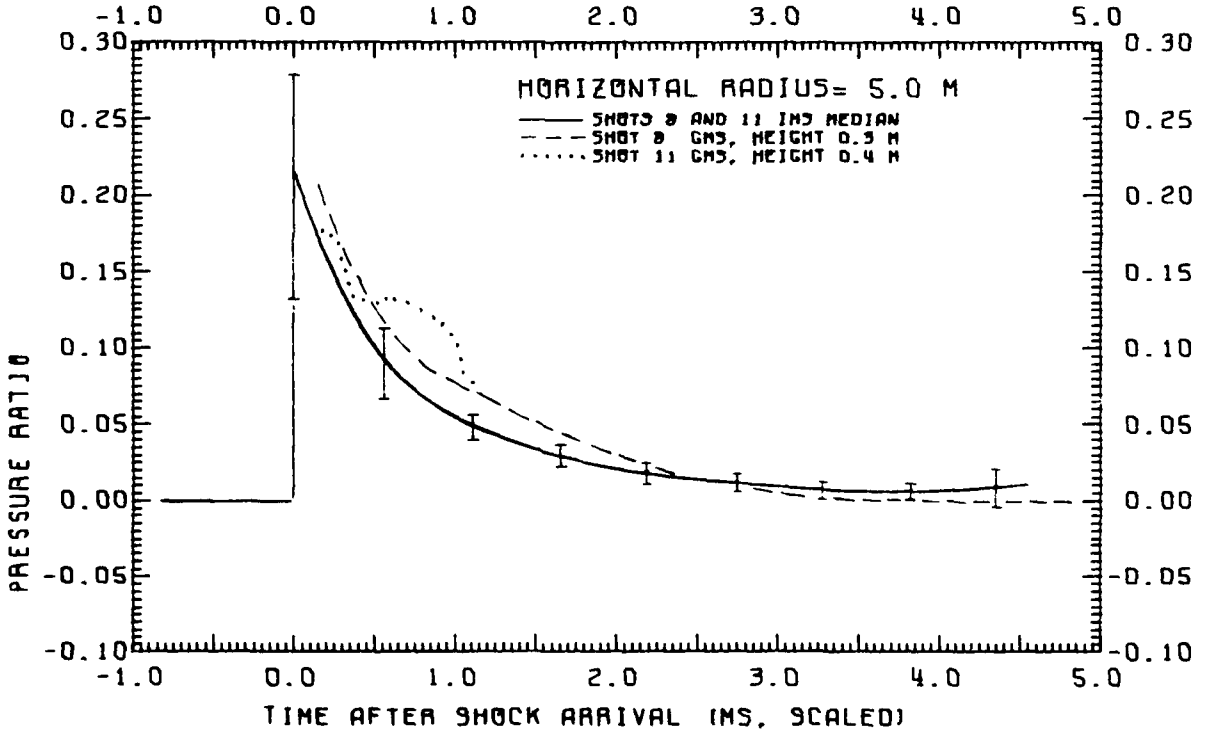

Figure 16B. Dynamic pressure time-histories.

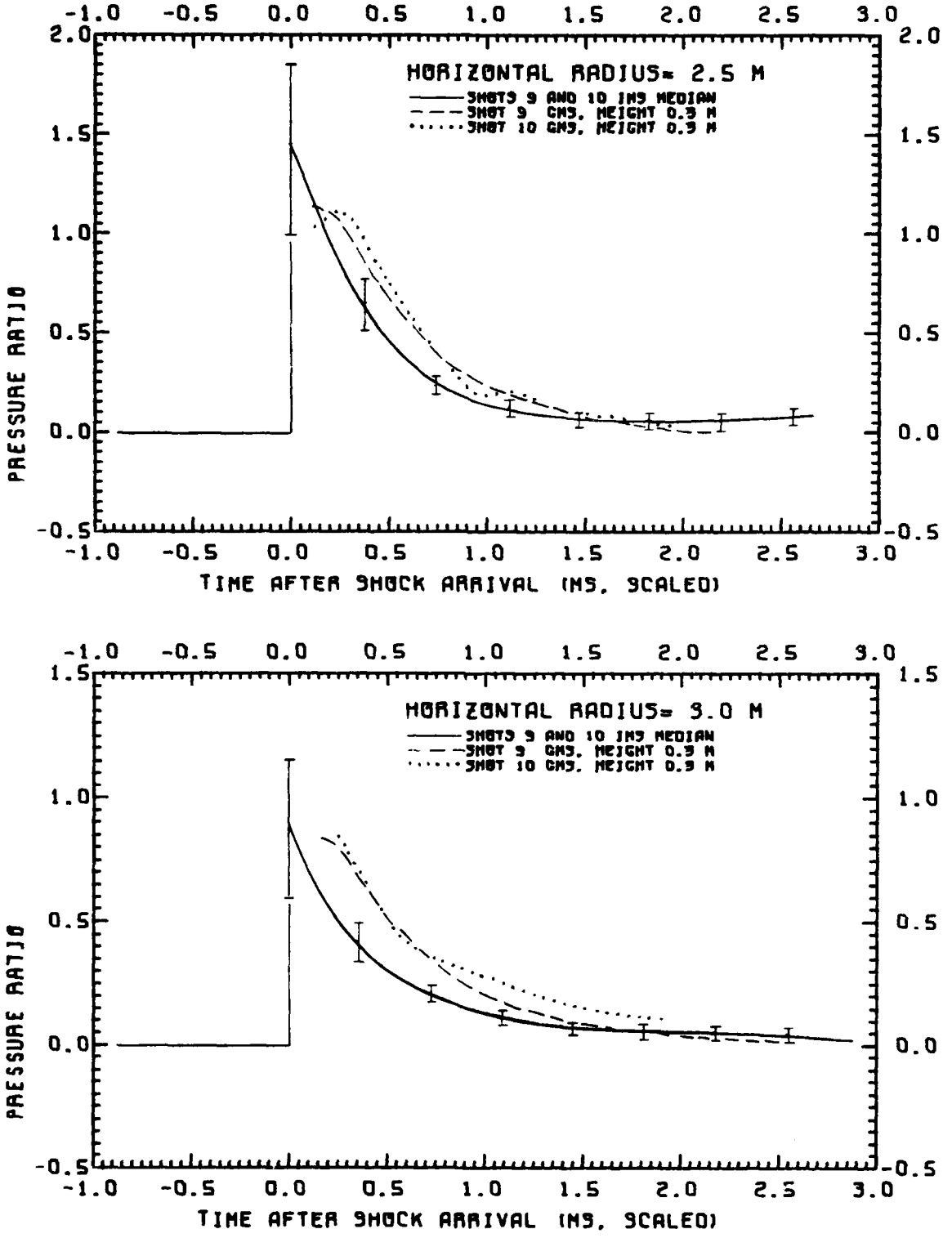

Figure 17. Dynamic pressure time-histories.

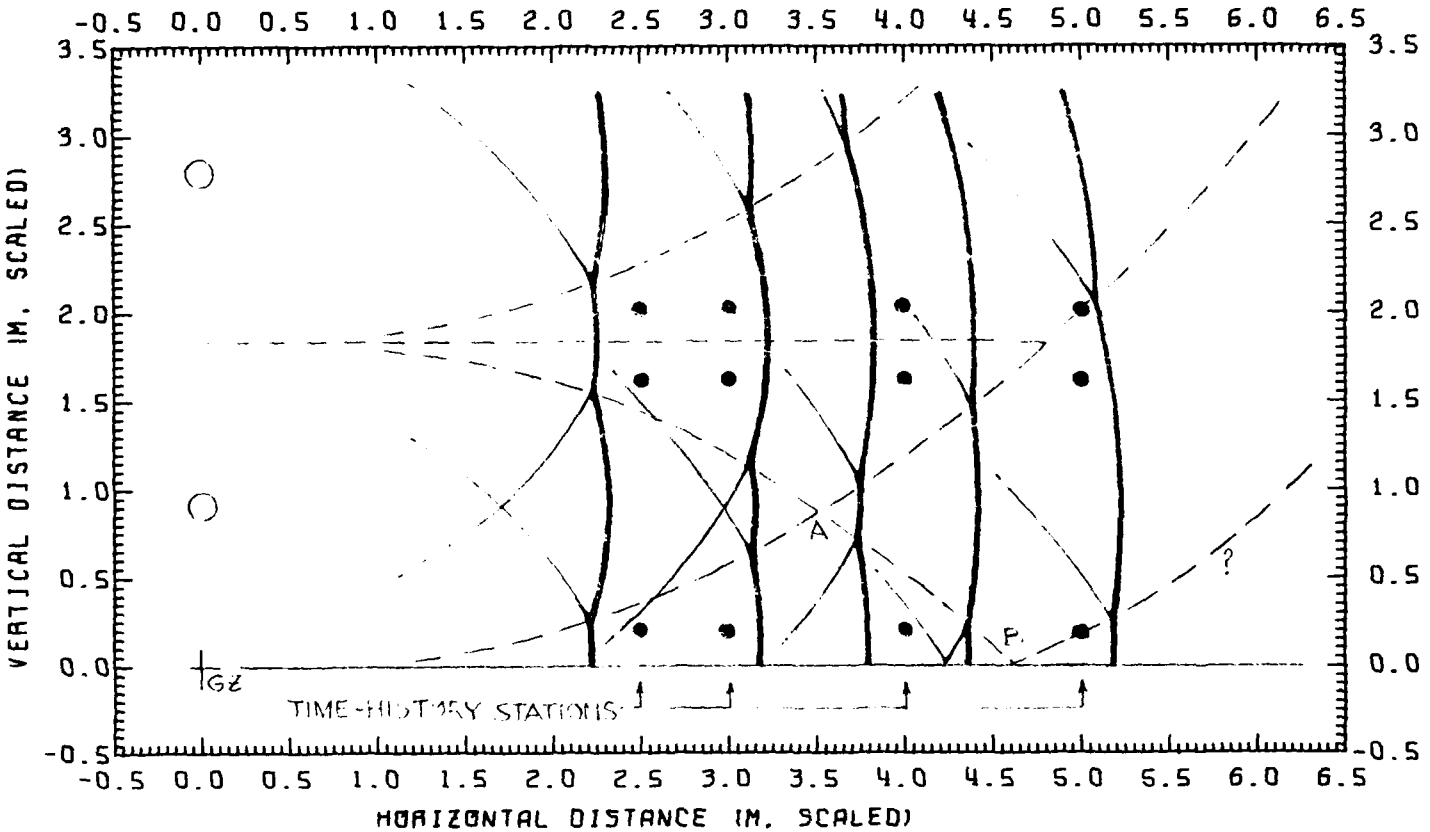

Figure 18. Shock front configuration map.

below the interaction plane. It is hoped that this question will be resolved in the future, following the analysis of the particle trajectories within Mach stem shocks produced by single explosions above the ground surface.

3-4 SURFACE CONTOURS.

In the four previous volumes of this series, the measurements of particle velocity, density, hydrostatic overpressure and dynamic pressure were also presented in the form of contours which mapped the appropriate physical property at fixed times after the detonation. On first inspection, it appears difficult to interpret these contours, some of which appear to be almost random in form. Nevertheless, when the contours from similar experiments are compared, there appears to be a high degree of repeatability in the results.

This is illustrated in Figure 19, in which the isotachs, namely, the contours joining points of equal particle velocity, are shown superposed for Shots 8 and 11 at scaled times of 2.5 ms, 4 ms, and 9 ms after detonation. A high degree of similarity in the two sets of contours can be seen, and this suggests that the plotting of experimentally measured contours is a valid method for comparing the flow fields from different experiments.

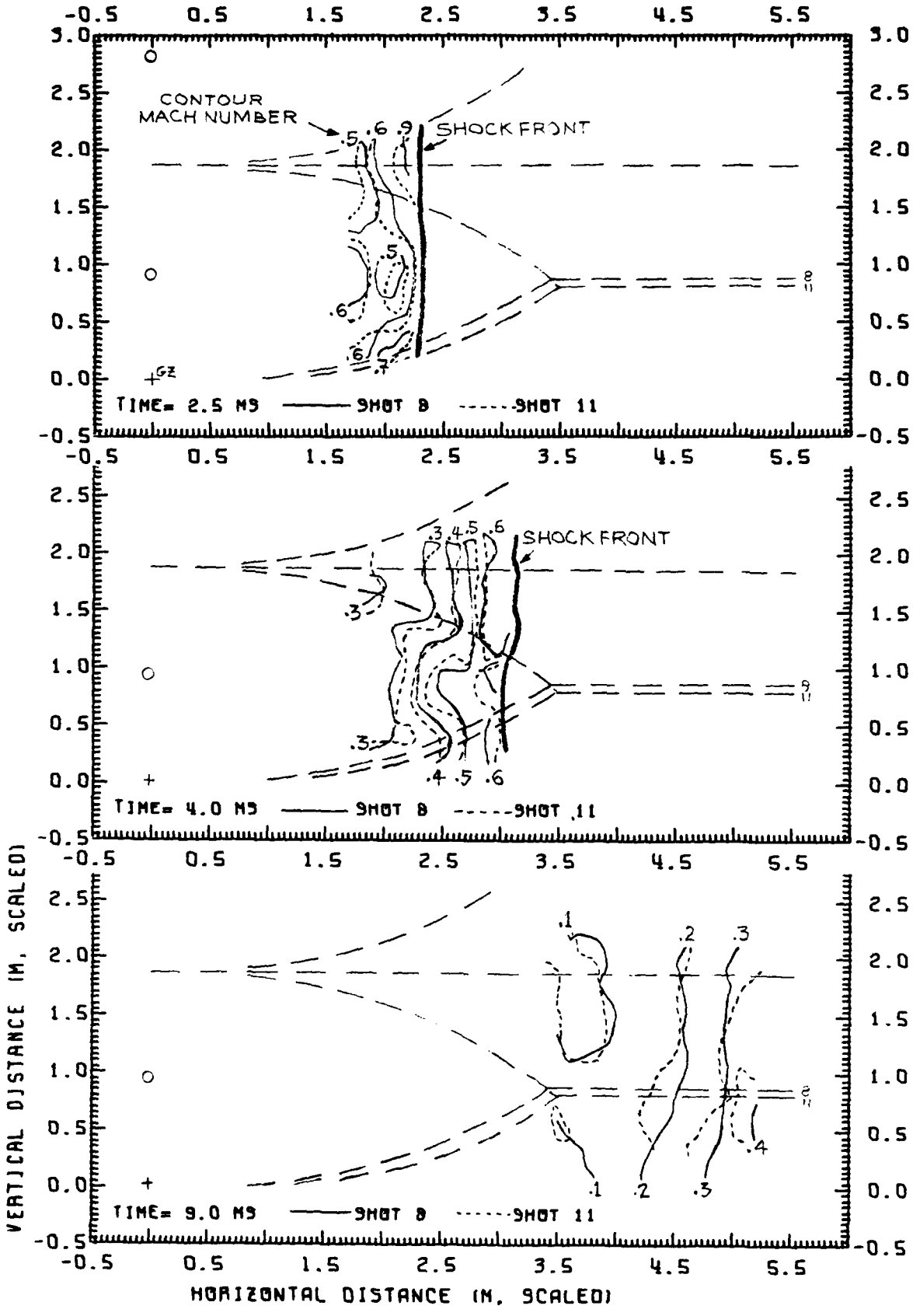

Figure 19. Particle velocity contour maps.

CHAPTER 4

CONCLUSIONS

Comparisons between the results obtained from the four dipole experiments presented in this report demonstrate complete consistency in the trajectories of the primary shocks from all eight explosions, indicating that they all detonated satisfactorily with equal energy yields. It should be stressed that this consistency is only apparent after the initial measurements have been scaled to allow for different atmospheric conditions. Even greater consistency after scaling might have been achieved if the exact masses of the individual charges had been known.

The measurements of the Mach stem blast waves above and below the interaction plane provide a set of "ideal" values against which to compare results of blast wave reflections from real ground surfaces. The "ideal" results should be of particular value for comparison with blast wave predictions made using numerical models, which normally assume shock reflections without energy loss or redistribution.

The results obtained from the particle trajectory analysis include the variation of Mach stem shock strength with distance, and the space and time variations of particle velocity, density, hydrostatic overpressure and dynamic pressure. Other physical properties within the blast waves such as entropy, temperature, sound speed and local Mach number can be provided if required.

The blast wave profiles in the ideal Mach stems at equal distances from the central axis for the two heights of burst are very similar, especially at larger distances.

The observed differences between the Mach stem shock strengths above the ground and at the interaction plane are similar to, but not as large as, those observed using refractive-image analysis. This implies both a height dependence and a variation in the shape of the Mach stem shock, and justifies further analysis.

Comparisons between the profiles of the blast waves over the ground and along the interaction plane show a consistent pattern in which the value

immediately behind the shock above the ground is normally less than at the interaction plane, but at later times the values above the ground are always larger than those at the interaction plane. This effect may be due to a lack of symmetry in the dipole experiments and not to ground surface effects. Analysis of the particle trajectories in blast waves from single air-burst charges should permit resolution of this point in the future.

SECTION 5

REFERENCES

5-1 Dewey, J.M., Classen, D.F., and McMillin, D.J., "Photogrammetry of the Shock Front Trajectories on DIPOLE WEST Shots 8, 9, 10 and 11," DNA 3777F, 1975.

5-2 Dewey, J.M., McMillin, D.J., and Trill, D., "Photogrammetry of the Particle Trajectories on DIPOLE WEST Shots 8, 9, 10 and 11," Volumes I through IV, as follows:

(a) Volume I, Shot 10, DNA 4326F-1 (1977)

(b) Volume II, Shot 9, DNA 4326F-2 (1977)

(c) Volume III, Shot 8, DNA 4326F-4 (1978)

(d) Volume IV, Shot 11, DNA 4326F-4 (1978).

DISTRIBUTION LIST

DEPARTMENT OF DEFENSE

Assistant to the Secretary of Defense
Atomic Energy
ATTN: Executive Assistant

Defense Advanced Rsch. Proj. Agency
ATTN: TIO

Defense Communications Agency
ATTN: CCTC, Code 510

Defense Technical Info. Center
12 cy ATTN: DD

Defense Intelligence Agency
ATTN: DI-7D
ATTN: DT-2
ATTN: DT-1C

Defense Nuclear Agency
ATTN: STSP
ATTN: SPAS
ATTN: SPTD
ATTN: SPSS
ATTN: DDST
4 cy ATTN: TITL

Field Command
Defense Nuclear Agency
ATTN: FCTMOT
ATTN: FCTMOF
ATTN: FCTMD
ATTN: FCPR

Field Command
Defense Nuclear Agency
Livermore Division
ATTN: FCPRL

Joint Strategic Tgt. Planning Staff
ATTN: JLTW-2
ATTN: JPTM

Undersecretary of Defense for Rsch. & Engrg.
ATTN: Strategic & Space Systems (OS)

DEPARTMENT OF THE ARMY

BMD Advanced Technology Center
Department of the Army
ATTN: ATC-T, M. Capps

BMD Systems Command
Department of the Army
ATTN: BMDSC-H, N. Hurst

Deputy Chief of Staff for Ops. & Plans
Department of the Army
ATTN: DAMO-NCZ

Deputy Chief of Staff for Rsch. Dev. & Acq.
Department of the Army
ATTN: DAMA-CSS-N

DEPARTMENT OF THE ARMY (Continued)

Harry Diamond Laboratories
Department of the Army
ATTN: DELHD-N-TF
ATTN: DELHD-N-P, J. Gwaltney

U.S. Army Ballistic Research Labs.
ATTN: DRDAR-BLV, W. Schuman, Jr.
ATTN: DRDAR-BLE, J. Keefer
ATTN: DRDAR-BL, R. Eichelberger
ATTN: DRDAR-BLV
ATTN: DRDAR-BLT, R. Vitali
ATTN: DRDAR-BLT, J. Frasier

U.S. Army Material & Mechanics Rsch. Ctr.
ATTN: DRXMR-HH, J. Dignam

U.S. Army Materiel Dev. & Readiness Cmd.
ATTN: DRCDE-D, L. Flynn

U.S. Army Missile R&D Command
ATTN: DRDMI-XS
ATTN: DRDMI-TKP, W. Thomas
ATTN: DRDMI-TRR, B. Gibson

U.S. Army Nuclear & Chemical Agency
ATTN: Library

U.S. Army TRADOC Systems Analysis Activity
ATTN: ATAA-TDC, R. Benson

DEPARTMENT OF THE NAVY

Naval Research Laboratory
ATTN: Code 6770, G. Cooperstein
ATTN: Code 2627
ATTN: Code 7908, A. Williams

Naval Sea Systems Command
ATTN: SEA-0352, M. Kinna

Naval Surface Weapons Center
ATTN: Code F31
ATTN: Code R15, J. Petes
ATTN: Code K06, C. Lyons

Naval Weapons Evaluation Facility
ATTN: P. Hughes
ATTN: L. Oliver

Office of Naval Research
ATTN: Code 465

Office of the Chief of Naval Operations
ATTN: OP 604E14, R. Blaise
ATTN: OP 604C
ATTN: OP 604C3, R. Piacesi

Strategic Systems Project Office
Department of the Navy
ATTN: NSP-272

DEPARTMENT OF THE AIR FORCE

Aeronautical Systems Division
Air Force Systems Command
2 cy ATTN: ASD/ENFTV, D. Ward

Air Force Flight Dynamics Laboratory
ATTN: FXG

Air Force Geophysics Laboratory
ATTN: LY, C. Touart

Air Force Materials Laboratory
ATTN: MBC, D. Schmidt
ATTN: MBE, G. Schmitt
ATTN: LLM, T. Nicholas

Air Force Rocket Propulsion Laboratory
ATTN: LKCP, G. Beale

Air Force Systems Command
ATTN: SOSS
ATTN: XRTO

Air Force Weapons Laboratory
Air Force Systems Command
ATTN: DYV, A. Sharp
ATTN: DYT
ATTN: DYV
ATTN: SUL
ATTN: DYS
ATTN: HO, W. Minge
2 cy ATTN: NTO

Arnold Engineering Development Center
Air Force Systems Command
ATTN: Library Documents

Deputy Chief of Staff
Operations, Plans and Readiness
Department of the Air Force
ATTN: AFXDOSS

Deputy Chief of Staff
Research, Development, & Acq.
Department of the Air Force
ATTN: AFRDQSM
ATTN: AFRD

Foreign Technology Division
Air Force Systems Command
ATTN: SDBG
ATTN: TQTD
ATTN: SDBS, J. Pumphrey

Headquarters Space Division
Air Force Systems Command
ATTN: DYS

Headquarters Space Division
Air Force Systems Command
ATTN: RST
ATTN: RSS
ATTN: RSSE

Ballistic Missile Office
Air Force Systems Command
ATTN: MNNH
ATTN: MNNR

DEPARTMENT OF THE AIR FORCE (Continued)

Strategic Air Command
Department of the Air Force
ATTN: DOXT
ATTN: XPQM
ATTN: XOBM
ATTN: XPFS

DEPARTMENT OF ENERGY

Department of Energy
ATTN: Document Control for OMA/RD&T

DEPARTMENT OF ENERGY CONTRACTORS

Sandia Laboratories
Livermore Laboratory
ATTN: Document Control for Library & Security Classification Div.
ATTN: Document Control for H. Norris, Jr.

Sandia Laboratories
ATTN: Document Control for T. Cook
ATTN: Document Control for M. Cowan
ATTN: Document Control for A. Chabai

DEPARTMENT OF DEFENSE CONTRACTORS

Acurex Corp.
ATTN: C. Nardo
ATTN: R. Rindal

Aerospace Corp.
ATTN: H. Blaes
ATTN: R. Strickler
ATTN: W. Mann
ATTN: R. Mortensen

Analytic Services, Inc.
ATTN: J. Selig

AVCO Research & Systems Group
ATTN: J. Stevens
ATTN: Document Control
ATTN: W. Broding
ATTN: J. Gilmore

Battelle Memorial Institute
ATTN: M. Vanderlind
ATTN: E. Unger

The Boeing Company
ATTN: P. Dyrdahl
ATTN: F. York
ATTN: D. Lempriere
ATTN: R. Holmes

Boeing Wichita Company
ATTN: C. Kwaney

Calspan Corp.
ATTN: M. Holden

DEPARTMENT OF DEFENSE CONTRACTORS (Continued)

Effects Technology, Inc.
ATTN: R. Parisse
ATTN: R. Wengler

General Electric Company
Space Division
ATTN: D. Edelman
ATTN: C. Anderson
ATTN: G. Harrison

General Electric Company
Re-Entry & Environmental Systems Div.
ATTN: P. Cline

General Electric Company-TEMPO
ATTN: DASIAC
5 cy ATTN: P. McMillin
5 cy ATTN: J. Dewey

General Research Corp.
ATTN: T. Stathacopoulos

Institute for Defense Analyses
ATTN: Classified Library
ATTN: J. Bengston

Ion Physics Corp.
ATTN: R. Evans

Kaman AviDyne
ATTN: R. Ruetenik
ATTN: E. Criscione
ATTN: N. Hobbs

Kaman Sciences Corp.
ATTN: D. Sachs
ATTN: J. Hoffman
ATTN: T. Meagher
ATTN: J. Keith
ATTN: F. Shelton

Lockheed Missiles & Space Co., Inc.
ATTN: R. Walz

Lockheed Missiles and Space Co., Inc.
ATTN: F. Borgardt

Martin Marietta Corp.
ATTN: G. Aiello
ATTN: J. Potts
ATTN: L. Kinnaird

McDonnell Douglas Corp.
ATTN: E. Fitzgerald
ATTN: J. Garibotti
ATTN: H. Berkowitz
ATTN: D. Dean
ATTN: L. Cohen
ATTN: P. Lewis, Jr.

National Academy of Sciences
National Materials Advisory Board
ATTN: D. Groves

Northrop Corp.
ATTN: D. Hicks

Pacific-Sierra Research Corp.
ATTN: G. Lang
ATTN: H. Brode

DEPARTMENT OF DEFENSE CONTRACTORS (Continued)

Physics International Company
ATTN: J. Shea

Prototype Development Associates, Inc.
ATTN: J. McDonald

R&D Associates
ATTN: P. Rausch
ATTN: J. Carpenter
ATTN: C. MacDonald
ATTN: W. Graham, Jr.
ATTN: F. Field

Rand Corp.
ATTN: J. Mate

Science Applications, Inc.
ATTN: D. Hove
ATTN: O. Nance
ATTN: J. Warner
ATTN: W. Yengst
ATTN: G. Ray

Science Applications, Inc.
ATTN: G. Burghart

Science Applications, Inc.
ATTN: W. Seebaugh
ATTN: W. Layson

Science Applications, Inc.
ATTN: A. Martellucci

Southern Research Institute
ATTN: C. Pears

SRI International
ATTN: D. Curran
ATTN: P. Dolan
ATTN: G. Abrahamson
ATTN: H. Lindberg

System Planning Corp.
ATTN: F. Adelman

Systems, Science & Software, Inc.
ATTN: G. Gurtman
ATTN: R. Duff

Terra Tek, Inc.
ATTN: S. Green

TRW Defense & Space Sys. Group
ATTN: P. Dai
ATTN: R. Plebuch
ATTN: G. Arenguren
ATTN: W. Wood
ATTN: P. Brandt
ATTN: D. Baer
ATTN: T. Williams
2 cy ATTN: I. Alber

TRW Defense & Space Sys. Group
ATTN: W. Polich
ATTN: L. Berger
ATTN: E. Allen
ATTN: V. Blankenship
ATTN: E. Wong